INTERNATIONAL JOURNAL OF
Robust and Nonlinear Control

Time-varying sliding mode controller for over-actuated systems with constrained and uncertain actuators in flight control applications

Note: The following files were submitted by the author for peer review, but cannot be converted to PDF. You must view these files (e.g. movies) online.

NJDnatbib.sty
References.bib
wileyNJD-AMA-NEW.aux
wileyNJD-AMA-NEW.bbl
wileyNJD-AMA-NEW.blg
wileyNJD-AMA-NEW.log
wileyNJD-AMA-NEW.pag
wileyNJD-AMA-NEW.synctex(1)
wileyNJD-AMA-NEW.synctex
wileyNJD-AMA-NEW.tex
WileyNJD-AMA.bst
WileyNJD-v2.cls

SCHOLARONE™
Manuscripts

ARTICLE TYPE

Time-varying sliding mode controller for over-actuated systems with constrained and uncertain actuators in flight control applications

Seyed Shahabaldin Tohidi*[1] | Yildiray Yildiz[2] | Ilya Kolmanovsky[3]

[1]Department of Applied Mathematics and Computer Science, Denmark Technical University, Lyngby, 2800 Kgs., Denmark
[2]Mechanical Engineering Department, Bilkent University, Ankara, 06800, Turkey
[3]Department of Aerospace Engineering, University of Michigan, Ann Arbor, MI 48109, USA

Correspondence
*Seyed Shahabaldin Tohidi, Department of Applied Mathematics and Computer Science, Denmark Technical University, Lyngby, 2800 Kgs., Denmark. Email: sshto@dtu.dk

Present Address
Seyed Shahabaldin Tohidi, Department of Applied Mathematics and Computer Science, Denmark Technical University, Lyngby, 2800 Kgs., Denmark.

Abstract

One solution to the problem of distributing the control action among redundant actuators with uncertain dynamics is employing an adaptive control allocator. This paper proposes a sliding mode controller which exploits a time-varying sliding surface to complement adaptive control allocation in the presence of actuator saturation. The proposed approach does not require error augmentation for tracking desired references, which diminishes the computational burden. Aerodata Model in Research Environment (ADMIRE), which is an over-actuated aircraft model, is adopted to demonstrate the efficacy of the proposed controller in simulation studies.

KEYWORDS:
sliding mode controller, control allocation, constrained systems, over-actuated systems

1 | INTRODUCTION

Redundancy in actuators is beneficial for improving functionality and fault tolerance of engineered systems. Such systems require an algorithm to distribute control signals among redundant actuators, which is referred to as control allocation. Systems where control allocation is employed include aircraft/spacecraft,[1,2,3,4,5,6,7,8,9,10] marine vessels,[11,12,13,14,15,16] automobiles,[17,18,19,20] robots,[21] and power systems.[22,23]

Control allocation methods can be categorized into the following categories: Pseudo-inverse-based methods, optimization-based methods, and dynamic control allocation. Pseudo-inverse-based control allocation methods[24,25,26,27] rely on manipulating the null space of the control input matrix, and have the lowest computational complexity. Optimization-based control allocation methods[28,29,30,31,32,33] solve an optimization problem at each time instant and can be computationally intense. In dynamic control allocation methods,[34,35,36,37,38,39,40] the control signals are distributed among actuators using a set of rules dictated by differential equations. A survey of control allocation methods can be found in Johansen et al.[41] In the presence of actuator uncertainty, the pseudo-inverse and optimization-based control allocation methods require fault detection and identification as well as persistency of excitation assumption for the input signals. Adaptive control allocation methods[35,36,37,40] on the other hand, can handle actuator uncertainties without the need for fault identification or persistency of excitation assumption.

Actuator limits can induce nonlinear behavior and lead to performance degradation, limit cycles, multiple equilibria, and even instability.[42,32,6,10] Several control allocation methods have been proposed in the literature that can handle actuator saturation. These include direct control allocation,[24] daisy chaining,[43] pseudo-inverse-based control allocation,[44] and iterative approaches

that use the null space of the control input matrix. [27] Optimization-based control allocation is another commonly used method of accounting for actuator magnitude and rate constraints. [28,29,31,13,1,6,45,46] Furthermore, a control allocation approach by Naderi et al, [47] employs model predictive control to handle actuator magnitude constraints. In order to allocate control signals in the presence of uncertainty as well as actuator constraints, an adaptive control allocator for constrained systems has been developed by Tohidi et al. [38,40] An adaptive control allocator which exploits a modified projection algorithm to handle magnitude and rate constraints in over-actuated systems is proposed by Tohidi et al. [48]

Although control allocation methods enable modularity for the overall control system design, as they separate the generation of the control signal and its distribution, control allocation errors can be significant in transients and degrade the performance. In vehicle and flight applications, the goal of the control allocation is to match the commanded (v) and the actual (Bu) control moments/forces, where u designates a vector of actuator positions. However, the equality $Bu = v$ may not be satisfied in the case of dynamic methods in transients or in the case of optimization-based methods if time to compute the solution online is insufficient. This transient control allocation error may not be negligible especially in the presence of actuator limits. Therefore, the controller must be designed to be robust to the control allocation error, as well as external disturbances. The robustness characteristics of the sliding mode control has motivated its use in combination with many control allocation implementations. [26,49,50]

An approach that employs a sliding mode controller together with a model predictive controller (MPC) has been considered to handle actuator constraints. [51,52,53,54] However, this combination leads to high computational complexity due to the need to solve an optimization problem online. Various other sliding mode control approaches have also been proposed which handle the constraints without using MPC. [55,56,57,58] However, these methods are developed for single input systems, unlike the one proposed in our paper for over-actuated systems.

Inspired by the work of Corradini et al. [59] this paper proposes a sliding mode controller with a time-varying sliding surface which guarantees stability and tracking, and which is robust not only to bounded disturbances but also to the adaptive control allocation error. Different from the work of Corradini et al, [59] the proposed controller solves the tracking problem in over-actuated constrained systems, in the presence of adaptive control allocation transients and disturbances, and in a simpler way by requiring only one design parameter. To the best of the authors knowledge, controllers that are robust to both the adaptive control allocator error and to external disturbances have not been proposed in the prior literature.

The initial results of this study were published in a conference paper by Tohidi et. al. [60] Differently from the conference version, this paper contains i) lemma and theorem proofs, ii) corollaries, detailed discussions and guidance regarding the initial condition selections, iii) simulation studies demonstrating the robustness of the controller even when sufficient conditions do not hold, and iv) discussions about the projection algorithm and the control allocation convergence set.

This paper is organized as follows. Section 2 describes the problem of controlling an over-actuated uncertain system in the presence of an adaptive control allocator. Section 3 presents the sliding mode controller design. The ADMIRE model is used in Section 4 to demonstrate the effectiveness of the proposed approach in the simulation environment. Finally, a summary is given in Section 5.

2 | PROBLEM STATEMENT AND PRELIMINARIES

We consider the adaptive control allocation setting in Figure 1 and the following Plant dynamics, [40]

$$\dot{x} = Ax + B_u(\Lambda u + d_u), \tag{1}$$

where $x \in \mathbb{R}^n$ is the state vector, $u = [u_1, ..., u_m]^T \in \mathbb{R}^m$ is the actuator input vector whose elements are constrained as $u_i \in [-u_{\max_i}, u_{\max_i}]$, $A \in \mathbb{R}^{n \times n}$ is a known state matrix, $B_u \in \mathbb{R}^{n \times m}$ is a known input matrix and $d_u \in \mathbb{R}^m$ is an unknown bounded disturbance input. The matrix $\Lambda \in \mathbb{R}^{m \times m}$ is assumed to be diagonal with positive elements representing actuator effectiveness uncertainty. It is assumed that the pair $(A, B_u\Lambda)$ is controllable. Due to actuator redundancy, the input matrix is rank deficient, that is $\text{Rank}(B_u) = \ell < m$. Consequently, B_u can be written as $B_u = B_v B$, where $B_v \in \mathbb{R}^{n \times \ell}$ is a full column rank matrix, i.e. $\text{Rank}(B_v) = \ell$, and $B \in \mathbb{R}^{\ell \times m}$. The decomposition of B_u helps exploit the actuator redundancy using control allocation. Employing this decomposition, (1) can be rewritten as

$$\dot{x} = Ax + B_v(B\Lambda u + \bar{d}), \tag{2}$$
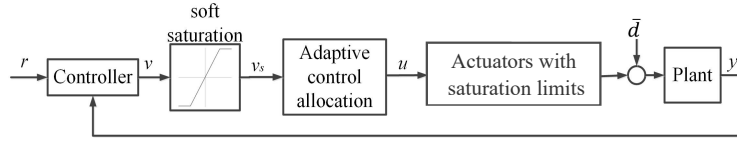
FIGURE 1 Block diagram of the closed loop system.

where $\bar{d}(t) = Bd_u(t)$ with an upper bound $||\bar{d}(t)|| \leq D$, for all $t \geq 0$. Throughout this paper, $||.||$ refers to the Euclidean norm for vectors and induced 2-norm for matrices. The control allocation task is to achieve

$$B\Lambda u + \bar{d} = v_s, \tag{3}$$

where $v_s \in \mathbb{R}^\ell$ is the output of the saturation block, which is receiving the control signal v as the input. (See Figure 1).

Considering the following dynamics,

$$\dot{y} = A_m y + B\Lambda u + \bar{d} - v_s, \tag{4}$$

where $A_m \in \mathbb{R}^{\ell \times \ell}$ is a stable matrix, a reference model is constructed as

$$\dot{y}_m = A_m y_m. \tag{5}$$

Defining the actuator input as a mapping from v_s to u,

$$u = \theta_v^T v_s, \tag{6}$$

where $\theta_v \in \mathbb{R}^{\ell \times m}$ represents the adaptive parameter matrix to be determined, and substituting (6) into (4), we obtain

$$\dot{y} = A_m y + (B\Lambda \theta_v^T - I_\ell)v_s + \bar{d}, \tag{7}$$

where I_ℓ is an identity matrix of dimension $\ell \times \ell$. It is assumed that there exists an ideal matrix θ_v^* such that

$$B\Lambda \theta_v^{*T} = I_\ell. \tag{8}$$

Defining $e = y - y_m$ and subtracting (5) from (7), it follows that

$$\dot{e} = A_m e + B\Lambda \tilde{\theta}_v^T v_s + \bar{d}, \tag{9}$$

where $\tilde{\theta}_v = \theta_v - \theta_v^*$.

Theorem 1. Consider (4) and (5). Suppose that the adaptive parameter matrix is updated using the adaptive law,

$$\dot{\theta}_v(t) = \Gamma_\theta \text{Proj}\left(\theta_v(t), -v_s(t)e^T(t)PB, f\right), \tag{10}$$

where the symmetric positive definite matrix P satisfies $A_m^T P + P A_m = -Q$, Q is a symmetric positive definite matrix, "Proj" is the projection operator[61,48] with a convex function $f \in C^1$, and $\Gamma_\theta = \gamma_\theta I_\ell$, where γ_θ is a positive scalar. Then, given any initial condition $e(0) \in \mathbb{R}^\ell$, $e(t)$ and $\tilde{\theta}_v(t)$ remain uniformly bounded for all $t \geq 0$ and their trajectories converge exponentially to the set

$$E_1 = \{(e, \tilde{\theta}_v) : ||e||^2 \leq \left(\frac{s\tilde{\theta}_{\max}^2}{\gamma_\theta \lambda_{\min}(Q)} + \frac{2\chi^4 D^2 ||Q||^2}{\sigma^2 \lambda_{\min}(Q)^2} \right) \frac{4s\chi^2 ||Q||}{\sigma \lambda_{\min}(Q)}, ||\tilde{\theta}_v|| \leq \tilde{\theta}_{max}\}, \tag{11}$$

where $s = -\min_i(\lambda_i(A_m + A_m^T)/2)$, $\sigma = -\max_i(\text{Real}(\lambda_i(A_m)))$, $\chi = \frac{3}{2}(1 + 4\frac{a}{\sigma})^{(\ell-1)}$, $a = ||A_m||$ and $||\tilde{\theta}_v(t)||_F \leq \tilde{\theta}_{max} \equiv \sqrt{\sum_{i,j}(\theta_{max_{i,j}} - \theta_{min_{i,j}} - \zeta_{i,j})^2}$. In addition, if $\bar{d}(t) = 0$ for $t \geq t'$ for some $t' \geq 0$, and $v_s(t)$ is uniformly continuous as a function of $t \in [t', +\infty)$, then $\lim_{t \to \infty} B\Lambda u(t) = v_s(t)$, i.e., (3) is achieved asymptotically.

Proof. See Tohidi et al.[40] 　　　　　　　　　　　　　　　　　　　　　　　　　　　　　□

The projection algorithm[61,48] employed in Theorem 1 exploits a continuous function $\text{Proj}(\theta_{v_{i,j}}, Y_{i,j}, f) : \mathbb{R} \times \mathbb{R} \times \mathcal{F} \to \mathbb{R}$ defined as

$$\text{Proj}(\theta_{v_{i,j}}, Y_{i,j}, f) \equiv \begin{cases} Y_{i,j} - Y_{i,j} f(\theta_{v_{i,j}}) & \text{if } f(\theta_{v_{i,j}}) > 0 \ \& \ Y_{i,j}(\frac{df}{d\theta_{v_{i,j}}}) > 0 \\ Y_{i,j} & \text{otherwise,} \end{cases} \tag{12}$$

where $Y_{i,j}$ is equal to $\dot{\theta}_{v_{i,j}}$ before being projected and $f(.) \in \mathcal{F}(\mathbb{R} \to \mathbb{R})$ is a convex and continuously differentiable (C^1) function given as

$$f(\theta_{v_{i,j}}) = \frac{(\theta_{v_{i,j}} - \theta_{min_{i,j}} - \zeta_{i,j})(\theta_{v_{i,j}} - \theta_{max_{i,j}} + \zeta_{i,j})}{(\theta_{max_{i,j}} - \theta_{min_{i,j}} - \zeta_{i,j})\zeta_{i,j}}, \tag{13}$$

and where $\zeta_{i,j}$ is the projection tolerance of the $(i,j)^{\text{th}}$ element of θ_v, which satisfies $0 < \zeta_{i,j} < 0.5(\theta_{max_{i,j}} - \theta_{min_{i,j}})$. $\theta_{max_{i,j}}$ and $\theta_{min_{i,j}}$ are the upper and lower bound of the $(i,j)^{\text{th}}$ element of θ_v. A step by step method for the determination of the projection bounds is given at Tohidi et al.[40]

By substituting (6) and (8) into (2), it follows that

$$\begin{aligned} \dot{x} &= Ax + B_v(B\Lambda u + \bar{d}) \\ &= Ax + B_v(B\Lambda \theta_v^T v_s + \bar{d}) \\ &= Ax + B_v(I + B\Lambda \tilde{\theta}_v^T)v_s + B_v\bar{d}. \end{aligned} \tag{14}$$

Defining $\Delta B(t) \equiv B\Lambda \tilde{\theta}_v^T(t)$, and substituting in (14), it follows that

$$\dot{x}(t) = Ax(t) + B_v(v_s(t) + d(t)), \tag{15}$$

where $d(t) = \Delta B(t)v_s(t) + \bar{d}(t) \in \mathbb{R}^\ell$ is the sum of the disturbance and the control allocation error. Therefore, the controller to be designed should be robust to both the disturbances *and* the control allocation errors. It is noted that since $\Delta B(t)$, $v_s(t)$ and $\bar{d}(t)$ are bounded, $d(t)$ is also bounded.

Thus far, we introduced the plant dynamics with constrained uncertain actuators, the adaptive control allocation algorithm, and the resulting system dynamics (15) after the inclusion of the control allocator. What remains to be done is the design of a controller that generates the signal v (see Figure 1). The controller needs to be robust to the control allocation error and the disturbances, in the presence of a software saturation. Note that software saturation is needed for the adaptive control allocator to provide a stable performance. In the proceeding sections, a sliding mode controller that satisfies these requirements is presented.

3 | CONTROLLER DESIGN

In this section, a design procedure for the controller that generates the virtual control signal v is proposed (see Figure 1).

The following two assumptions are made:

Assumption 1. The dynamics in (15) can be written as

$$\begin{bmatrix} \dot{x}^{(1)} \\ \dot{x}^{(2)} \end{bmatrix} = \begin{bmatrix} A_{1,1} & A_{1,2} \\ A_{2,1} & A_{2,2} \end{bmatrix} \begin{bmatrix} x^{(1)} \\ x^{(2)} \end{bmatrix} + B_v(v_s + d), \tag{16}$$

where $A_{1,1} \in \mathbb{R}^{(n-\ell)\times(n-\ell)}$ is a Hurwitz matrix, $A_{1,2} \in \mathbb{R}^{(n-\ell)\times\ell}$, $A_{2,1} \in \mathbb{R}^{\ell\times(n-\ell)}$ and $A_{2,2} \in \mathbb{R}^{\ell\times\ell}$ are parts of the state matrix, and $x^{(1)} \in \mathbb{R}^{(n-\ell)}$ and $x^{(2)} \in \mathbb{R}^\ell$ constitute the state vector. It is noted that the elements of the state matrix, $A_{i,j}, i = 1, 2, j = 1, 2$, are known. We are interested in the vector $x^{(2)}$ as the system output y. Therefore,

$$y = C \begin{bmatrix} x^{(1)} \\ x^{(2)} \end{bmatrix}, \tag{17}$$

where $C = [0_{\ell\times(n-\ell)} \ I_\ell]$.

Assumption 2. The matrix $B_v \in \mathbb{R}^{n\times\ell}$ is in the form $[0_{\ell\times(n-\ell)} \ I_\ell]^T$.

Remark 1. Although the proposed controller can be applied to other dynamical systems satisfying Assumptions 1 and 2, the above assumptions are justified for typical aircraft models,[2,62] which are the main focus of this paper. In the simulation section, these assumptions are validated for the AeroData Model in Research Environment (ADMIRE).[29,1]

Remark 2. For systems where Assumption 2 does not hold, given that B_v has full column rank, it is possible to find a transformation matrix, T_B, such that $\hat{B}_v = T_B B_v = [0_{\ell \times (n-\ell)} \; I_\ell]^T$.[59,63] However, employing this transformation may lead to a state space realization which violates Assumption 1.

Remark 3. Since $A_{1,1}$ is assumed to be Hurwitz, showing that the states $x^{(2)}$ are bounded will be sufficient to demonstrate the boundness of $x^{(1)}$.

3.1 | Time Varying Sliding Surface

The sliding surface, inspired by[59], is given as

$$s(x^{(2)}(t), x^{(2)}(t_0), t) = x^{(2)}(t) - x^{(2)}(t_0)e^{-\bar{\lambda}(t-t_0)} - \frac{2}{\pi}r(t)\tan^{-1}\left(\bar{\lambda}(t-t_0)\right) = 0, \tag{18}$$

where $\bar{\lambda} > 0$ is a scalar parameter, $x^{(2)} \in \mathbb{R}^\ell$ is defined in (16), and $r(t) \in \mathbb{R}^\ell$ is the twice continuously differentiable (C^2) reference to be tracked.

The response of a system controlled by a sliding mode controller includes two phases.[64] The first phase is called the reaching phase. During this phase, the controller drives the system towards the sliding surface. In the second phase, which is called the sliding phase, the trajectories evolve on the sliding manifold. For the sliding surface (18), no reaching phase exists since the sliding surface is a function of the initial condition and the trajectories are on the sliding surface at $t = t_0$, i.e. $s(x^{(2)}(t), x^{(2)}(t_0), t_0) = 0$. These types of sliding surfaces belong to the family of integral sliding surfaces.[65] Below, we analyze the behavior of the system trajectories on the sliding surface and show that the trajectories remain on the sliding surface for all $t \geq t_0$.

3.2 | Motion on the sliding surface

Using (18), the trajectories of $x^{(2)}$ on the sliding surface satisfy

$$x^{(2)}(t) = x^{(2)}(t_0)e^{-\bar{\lambda}(t-t_0)} + \frac{2}{\pi}r(t)\tan^{-1}\left(\bar{\lambda}(t-t_0)\right). \tag{19}$$

Substituting (19) into (16), it follows that

$$\dot{x}^{(1)} = A_{1,1}x^{(1)} + A_{1,2}\left(x^{(2)}(t_0)e^{-\bar{\lambda}(t-t_0)} + \frac{2}{\pi}r(t)\tan^{-1}\left(\bar{\lambda}(t-t_0)\right)\right). \tag{20}$$

By defining $G_1 \equiv A_{1,2}x^{(2)}(t_0)$, and $G_2(t) \equiv \frac{2}{\pi}A_{1,2}r(t)\tan^{-1}(\bar{\lambda}(t-t_0))$, (20) can be rewritten as

$$\dot{x}^{(1)} = A_{1,1}x^{(1)} + G_1 e^{-\bar{\lambda}(t-t_0)} + G_2(t) = A_{1,1}x^{(1)} + g(t), \tag{21}$$

where $g(t) \equiv G_1 e^{-\bar{\lambda}(t-t_0)} + G_2(t)$.

Lemma 1. When $x^{(2)}(t)$ is on the sliding surface (18), $||x^{(1)}(t)|| \leq k\bar{x}^{(1)}(t_0) + K_2\bar{x}^{(2)}(t_0) + K_2\bar{r}$, where $K_2 = \frac{k}{\xi}||A_{1,2}||$, k and ξ are positive constants, and $\bar{x}^{(1)}(t_0)$, $\bar{x}^{(2)}(t_0)$ and $\bar{r}$ are the upper bounds of $||x^{(1)}(t_0)||$, $||x^{(2)}(t_0)||$ and $||r(t)||$, respectively. Furthermore, $\lim_{t\to\infty} y(t) = r(t)$.

Proof. Per Assumption 1, $A_{1,1}$ is Hurwitz, hence the homogeneous system $\dot{x}_h^{(1)}(t) = A_{1,1}x_h^{(1)}(t)$ is globally exponentially stable at the origin. The solution of this system is given as $x_h^{(1)}(t) = \Phi(t, t_0)x_h^{(1)}(t_0)$, where $\Phi(t, t_0)$ is the state transition matrix and there exist constants $k > 0$ and $\xi > 0$ such that

$$||\Phi(t, t_0)|| \leq ke^{-\xi(t-t_0)}, \quad \forall t \geq t_0, \tag{22}$$

where $\xi = \frac{1}{2||X||}$, $k = \sqrt{||X^{-1}||||X||}$ and the positive definite matrix $X \in \mathbb{R}^{(n-\ell)\times(n-\ell)}$ satisfies the Lyapunov equation $A_{1,1}^T X + X A_{1,1} = -I_{n-\ell}$.[66]

Since the state transition matrices of the dynamics $\dot{x}_h^{(1)}(t) = A_{1,1}x_h^{(1)}(t)$ and $\dot{x}^{(1)}(t) = A_{1,1}x^{(1)}(t) + g(t)$ are the same, we use the state transition matrix $\Phi(t, t_0)$ used in (22) to provide the solution of (21) as

$$x^{(1)}(t) = \Phi(t, t_0)x^{(1)}(t_0) + \int_{t_0}^t \Phi(t, \eta)g(\eta)d\eta. \tag{23}$$

Taking the norm of both sides of (23) and using the triangle inequality, we obtain that

$$||x^{(1)}(t)|| \leq ||\Phi(t,t_0)x^{(1)}(t_0)|| + \int_{t_0}^{t} ||\Phi(t,\eta)||||g(t)||d\eta. \tag{24}$$

Using the definition of $g(t)$, given after (21), it follows that $||g(t)|| = ||G_1 e^{-\bar{\lambda}t} + G_2(t)|| \leq ||G_1|| + \sup_{t \geq t_0} ||G_2(t)||$. Note that, since $G_2(t)$ is a function of the reference input $r(t)$, $\sup_{t \geq t_0} ||G_2(t)||$ exists (see the definition of G_2 given after (20)). Therefore, $||g(t)|| \leq ||A_{1,2}||\bar{x}^{(2)}(t_0) + ||A_{1,2}||\bar{r}$. Defining $K_1 = ||A_{1,2}||\bar{x}^{(2)}(t_0) + ||A_{1,2}||\bar{r}$, and using (22), (24) can be rewritten as,

$$||x^{(1)}(t)|| \leq k\bar{x}^{(1)}(t_0)e^{-\xi(t-t_0)} + kK_1 \int_{t_0}^{t} e^{-\xi(t-\eta)}d\eta$$

$$\leq k\bar{x}^{(1)}(t_0)e^{-\xi(t-t_0)} + kK_1\frac{1}{\xi}\left(1 - e^{-\xi(t-t_0)}\right)$$

$$\leq k\bar{x}^{(1)}(t_0) + kK_1\frac{1}{\xi}$$

$$= k\bar{x}^{(1)}(t_0) + k\left(||A_{1,2}||\bar{x}^{(2)}(t_0) + ||A_{1,2}||\bar{r}\right)\frac{1}{\xi}$$

$$\leq k\bar{x}^{(1)}(t_0) + K_2\bar{x}^{(2)}(t_0) + K_2\bar{r}, \tag{25}$$

where $K_2 = \frac{k}{\xi}||A_{1,2}||$, and $\bar{x}^{(1)}(t_0)$ and $\bar{x}^{(2)}(t_0)$ represent the upper bounds on $||x^{(1)}(t_0)||$ and $||x^{(2)}(t_0)||$, respectively. Since the reference signal $r(t)$, $x^{(1)}(t_0)$ and $x^{(2)}(t_0)$ are bounded, (25) shows that $x^{(1)}(t)$ is bounded. Since $x(t_0)$ and $r(t)$ are bounded, it can be shown, using (19), that $x^{(2)}(t)$ is bounded and converges to $r(t)$. Since $y = x^{(2)}$, this completes the proof. □

3.3 | Control Law

Figure 1 shows that once the control signal v is generated by the controller, it is passed through a software saturation block, whose output is represented by v_s. In this subsection, it is assumed that $v_s = v$ to demonstrate that with the proposed control law, trajectories stay on (18) and hence properties of Lemma 1 hold. This requires that v always stays within saturation bounds. A condition for this assumption to hold will be presented in the next subsection.

Definition 1. $\text{sign}_v(a)$, where a is a column vector, is a diagonal matrix whose elements are the signs of the elements of the vector a. For example, $\text{sign}_v([a_1 \ a_2]^T) = \text{diag}(\text{sign}(a_1), \ \text{sign}(a_2))$, where a_1 and a_2 are scalars.

Definition 2. $|a|_v \equiv \text{sign}_v(a)a$ and $|a^T|_v \equiv a^T\text{sign}_v(a)$, where a is a column vector and $\text{sign}_v(.)$ is defined in Definition 1. For example, $|[a_1 \ a_2]|_v = [a_1 \ a_2]\text{sign}_v([a_1 \ a_2]^T) = [|a_1| \ |a_2|]$, where a_1 and a_2 are scalars.

Theorem 2. Consider the dynamics in (16) with the control law,

$$v(t) = -A_{2,1}x^{(1)}(t) - A_{2,2}x^{(2)}(t) - \bar{\lambda}x^{(2)}(0)e^{-\bar{\lambda}t} + \frac{2}{\pi}\dot{r}(t)\tan^{-1}(\bar{\lambda}t) + \frac{2}{\pi}r(t)\frac{\bar{\lambda}}{1 + \bar{\lambda}^2t^2} - \text{sign}_v\left(s(x^{(2)}(t), x^{(2)}(0), t)\right)\rho, \tag{26}$$

where $\rho \in R^r$ contains the absolute upper bounds of the elements of the disturbance vector d, and $s(x^{(2)}(t), x^{(2)}(0), t)$ is the sliding surface (18). Assume $v_s(t) = v(t)$ for all t. Then, the trajectories of $x^{(2)}$ stay on the sliding surface (18).

Proof. Consider a Lyapunov function candidate $V_2(s) = \frac{1}{2}s^Ts$, where the arguments of $s(x^{(2)}(t), x^{(2)}(t_0), t)$ are dropped for clarity. By taking the time-derivative of V_2 along the system trajectories, and using (18) with $t_0 = 0$, we obtain

$$\dot{V}_2 = s^T\dot{s} = s^T\left(\dot{x}^{(2)}(t) + \bar{\lambda}x^{(2)}(0)e^{-\bar{\lambda}t} - \frac{2}{\pi}\dot{r}(t)\tan^{-1}(\bar{\lambda}t) - \frac{2}{\pi}r(t)\frac{\bar{\lambda}}{1 + \bar{\lambda}^2t^2}\right). \tag{27}$$

Using (16) and Assumption 2, we have $\dot{x}^{(2)}(t) = A_{2,1}x^{(1)}(t) + A_{2,2}x^{(2)}(t) + v + d$. Therefore, (27) can be rewritten as

$$\dot{V}_2 = s^T\left(A_{2,1}x^{(1)}(t) + A_{2,2}x^{(2)}(t) + v + d + \bar{\lambda}x^{(2)}(0)e^{-\bar{\lambda}t} - \frac{2}{\pi}\dot{r}(t)\tan^{-1}(\bar{\lambda}t) - \frac{2}{\pi}r(t)\frac{\bar{\lambda}}{1 + \bar{\lambda}^2t^2}\right). \tag{28}$$

By substituting the control law (26) into (28), and using Definitions 1 and 2, it follows that

$$\dot{V}_2 = s^T[d - \text{sign}_v(s)\rho] = s^Td - |s^T|_v\rho \leq |s^T|_v(|d|_v - \rho). \tag{29}$$

Since the elements of $|d|_v - \rho$ are non-positive, $\dot{V}_2 \leq 0$. Therefore, $x^{(2)}$ trajectories, which are on the sliding surface at $t = t_0$, will remain there for all $t > 0$. ☐

3.4 | Bounding the control signals

In this section, we provide a method, inspired by the work of Corradini et al,[59] to make sure that $|v_i| \leq M_i$, where v_i refers to the ith element of the control signal v, and M_i is a positive scalar, $i = 1, 2, ..., \ell$, which is a predefined soft saturation limit. This ensures that $v_s = v$, which is an assumption used in the previous section. Note that the values of M_i are calculated using the information about actuator constraints and the control matrix. The actuator constraints are $u(t) \in \Omega_u = \{[u_1, ..., u_m]^T : u_{min_i} \leq u_i \leq u_{max_i}, i = 1, ..., m\}$. Using Ω_u, the set Ω_v, defining all realizable values of the control input v, can be obtained as $\Omega_v = \{v : v = Bu, u \in \Omega_u, B^\dagger v \in \Omega_u\}$, where $(.)^\dagger$ refers to the pseudo inverse of a non-square matrix. Furthermore, there exist $M_i, i = 1, ..., r$, such that $\hat{\Omega}_v \equiv \{v : v_i \in [-M_i, M_i], i = 1, ..., r\} \subset \Omega_v$. The set $\hat{\Omega}_v$ can be used to define the constraints which are enforced using a soft saturation function.[40]

We have observed in our simulation studies that the controller is robust for a range of cases where the assumption in Section 3.3 is violated. However, to have formal stability guarantees, we present sufficient conditions in this section that can be used to ensure that $v_s = v$. Later in the simulations section, we show that these conditions are indeed sufficient, not necessary, and even when they are violated good closed-loop performance is maintained.

Lemma 2. The control signals $v_i, i = 1, 2, ..., \ell$, are bounded by $M_i, i = 1, 2, ..., \ell$, i.e. $|v_i(t)| \leq M_i$ for all t if the inequality

$$\left| -\sum_{\omega=1}^{n-\ell}\sum_{j=1}^{n-\ell} a_{2_{i,\omega}}\phi_{\omega,j}(t)x_j^{(1)}(0) - \int_0^t \left(\sum_{\omega=1}^{n-\ell}\sum_{j=1}^{n-\ell} a_{2_{i,\omega}}\phi_{\omega,j}(t-\eta) \left[\sum_{k=n-\ell+1}^{n} a_{1_{j,k}} \left(x_{k-n+\ell}^{(2)}(0)e^{-\bar{\lambda}\eta} + r_{k-n+\ell}(\eta)\frac{2}{\pi}\tan^{-1}(\bar{\lambda}\eta) \right) \right] \right) d\eta \right.$$

$$\left. -\sum_{j=n-\ell+1}^{n} a_{2_{i,j}} \left(x_{j-n+\ell}^{(2)}(0)e^{-\bar{\lambda}t} + \frac{2}{\pi}r_{j-n+\ell}(t)\tan^{-1}(\bar{\lambda}t) \right) - \bar{\lambda}x_{n-\ell+i}(0)e^{-\bar{\lambda}t} + \frac{2}{\pi}\dot{r}_i(t)\tan^{-1}(\bar{\lambda}t) + \frac{2}{\pi}r_i(t)\frac{\bar{\lambda}}{1+\bar{\lambda}^2t^2} \right| \leq M_i - \rho_i, \quad (30)$$

where $i = 1, ..., \ell$, is satisfied for all $t \geq 0$, where ρ is defined in Theorem 2, and $\phi_{i,j}(t)$ is the $(i, j)^{\text{th}}$ element of the state transition matrix $\Phi(t, t_0)$ in (22), with $t_0 = 0$.

Proof. See Appendix A. ☐

Remark 4. For (30) to be mathematically meaningful, its right hand side, $M_i - \rho_i$, must be positive. It is shown in Tohidi et al.[40] that this is indeed the case.

The adjustable parameters in (30) are the initial values of the states $x(0) = [x^{(1)^T}(0), x^{(2)^T}(0)]^T$ and the scalar design parameter $\bar{\lambda}$. Assuming that the reference, $r(t)$, input vector and its rate of change are bounded, all of the terms in (30) are either bounded or converge to zero. Since $A_{1,1}$ is stable, the elements of state transition matrix, $\phi_{i,j}(t)$, converge to zero exponentially fast (see (22)). Specifically for the investigated flight control problem, the state transition matrix of $x^{(1)}$ dynamics (see (1)), where $x^{(1)} = [\alpha, \beta]^T$ and α and β are the angle of attack and the sideslip angle, respectively, consists of sums of decaying exponentials due to distinct eigenvalues. In this case, calculating the feasible values of the adjustable parameters becomes easier since the inequality (30) takes a simpler form, which is explained in the following corollary.

Corollary 1. If the elements of the state transition matrix are formed as sums of exponential functions (which is the case in several flight control problems), that is, $\phi_{i,j}(t) = \sum_{\kappa=1}^{\bar{n}} c_{i,j_\kappa} e^{-h_{i,j_\kappa}t}$ with $h_{i,j_\kappa} > 0$ and $\bar{n}$ a positive integer, then the control signals $v_i, i = 1, ..., \ell$ are bounded by $M_i, i = 1, ..., \ell$, i.e. $|v_i| \leq M_i$ if the inequality

$$W_i \equiv \left| -\sum_{\omega=1}^{n-\ell}\sum_{j=1}^{n-\ell}\sum_{\kappa=1}^{\bar{n}} a_{2_{i,\omega}}c_{\omega,j_\kappa}e^{-h_{\omega,j_\kappa}t}x_j^{(1)}(0) - \sum_{\omega=1}^{n-\ell}\sum_{j=1}^{n-\ell}\sum_{\kappa=1}^{\bar{n}}\sum_{k=n-\ell+1}^{n} a_{2_{i,\omega}}c_{\omega,j_\kappa}a_{1_{j,k}}x_{k-n+\ell}^{(2)}(0)q_{\omega,j_\kappa}(t) \right.$$

$$\left. -\sum_{j=n-\ell+1}^{n} a_{2_{i,j}} \left(x_i^{(2)}(0)e^{-\bar{\lambda}t} + \frac{2}{\pi}r_i(t)\tan^{-1}(\bar{\lambda}t) \right) - \bar{\lambda}x_{n-\ell+i}(0)e^{-\bar{\lambda}t} + \frac{2}{\pi}\dot{r}_i(t)\tan^{-1}(\bar{\lambda}t) + \frac{2}{\pi}r_i(t)\frac{\bar{\lambda}}{1+\bar{\lambda}^2t^2} \right.$$

$$\left. + \int_0^t \sum_{\omega=1}^{n-\ell}\sum_{j=1}^{n-\ell}\sum_{\kappa=1}^{\bar{n}}\sum_{k=n-\ell+1}^{n} -a_{2_{i,\omega}}c_{\omega,j_\kappa}e^{-h_{\omega,j_\kappa}(t-\eta)}a_{1_{j,k}}r_{k-n+\ell}(\eta)\frac{2}{\pi}\tan^{-1}(\bar{\lambda}\eta)d\eta \right| \leq M_i - \rho_i, \quad i = 1, ..., \ell, \quad (31)$$
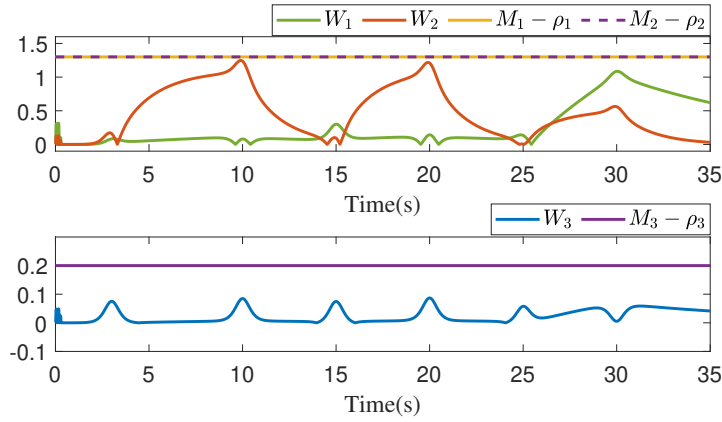
FIGURE 2 Validation of the inequality (31).

where

$$
q_{\omega,j_\kappa}(t) \equiv \begin{cases} te^{-h_{\omega,j_\kappa}t}, & \bar{\lambda} = h_{\omega,j_\kappa}, \\ \dfrac{e^{-\bar{\lambda}t} - e^{-h_{\omega,j_\kappa}t}}{h_{\omega,j_\kappa} - \bar{\lambda}}, & \bar{\lambda} \neq h_{\omega,j_\kappa}, \end{cases} \tag{32}
$$

is satisfied for all $t \geq 0$.

Proof. See Appendix B. □

*Remark 5.* Given the upper and lower bounds of the reference signals and their derivatives, such that $r_i(t) \in [r_i^-, r_i^+]$ and $\dot{r}_i(t) \in [\dot{r}_i^-, \dot{r}_i^+]$, $r_i^- = -r_i^+$, $\dot{r}_i^- = -\dot{r}_i^+$, one way to check the inequality (31) is by using the triangle inequality and finding an upper bound for W_i as $\sum_{\omega=1}^{n-\ell} \sum_{j=1}^{n-\ell} \sum_{\kappa=1}^{\bar{n}} |a_{2_{i,\omega}} c_{\omega,j_\kappa} x_j^{(1)}(0)| + \sum_{\omega=1}^{n-\ell} \sum_{j=1}^{n-\ell} \sum_{\kappa=1}^{\bar{n}} \sum_{k=n-\ell+1}^{n} |a_{2_{i,\omega}} c_{\omega,j_\kappa} a_{1_{j,k}} x_{k-n+\ell}^{(2)}(0) \bar{q}_{\omega,j_\kappa}| + \sum_{j=n-\ell+1}^{n} |a_{2_{i,j}}(x_i^{(2)}(0))| + \sum_{j=n-\ell+1}^{n} |a_{2_{i,j}} r_i^+| + |\bar{\lambda} x_{n-\ell+i}(0)| + |\dot{r}_i^+| + |\frac{2}{\pi} r_i^+ \bar{\lambda}| + \sum_{\omega=1}^{n-\ell} \sum_{j=1}^{n-\ell} \sum_{\kappa=1}^{\bar{n}} \sum_{k=n-\ell+1}^{n} |a_{2_{i,\omega}} c_{\omega,j_\kappa} a_{1_{j,k}} \frac{r_{k-n+\ell}^+}{h_{\omega,j_\kappa}}| \leq M_i - \rho_i$, where $\bar{q}_{\omega,j_\kappa} = \max\{e^{-1} h_{\omega,j_\kappa}^{-1}, \frac{2}{|h_{\omega,j_\kappa} - \bar{\lambda}|}\}$. This inequality can be simplified as $W_{i,1} + \bar{\lambda} W_{i,2} \leq 0$, where $W_{i,1} = \sum_{\omega=1}^{n-\ell} \sum_{j=1}^{n-\ell} \sum_{\kappa=1}^{\bar{n}} |a_{2_{i,\omega}} c_{\omega,j_\kappa} x_j^{(1)}(0)| + \sum_{\omega=1}^{n-\ell} \sum_{j=1}^{n-\ell} \sum_{\kappa=1}^{\bar{n}} \sum_{k=n-\ell+1}^{n} |a_{2_{i,\omega}} c_{\omega,j_\kappa} a_{1_{j,k}} x_{k-n+\ell}^{(2)}(0) q_{\omega,j_\kappa}(t)| + \sum_{j=n-\ell+1}^{n} |a_{2_{i,j}}(x_i^{(2)}(0))| + \sum_{j=n-\ell+1}^{n} |a_{2_{i,j}} r_i^+| + |\dot{r}_i^+| + \sum_{\omega=1}^{n-\ell} \sum_{j=1}^{n-\ell} \sum_{\kappa=1}^{\bar{n}} \sum_{k=n-\ell+1}^{n} |a_{2_{i,\omega}} c_{\omega,j_\kappa} a_{1_{j,k}} \frac{r_{k-n+\ell}^+}{h_{\omega,j_\kappa}}| - M_i + \rho_i$ and $W_{i,2} = |x_{n-\ell+i}(0)| + |\frac{2}{\pi} r_i^+|$. Note that $W_{i,1}$ and $W_{i,2}$ are functions of $x^{(1)}(0)$, $x^{(2)}(0)$ and r_i^+, and remain constant along the closed-loop trajectory. Since $W_{i,2}$ is positive, a value of $\bar{\lambda} > 0$ satisfying $W_{i,1} + \bar{\lambda} W_{i,2} \leq 0$ can always be found if $W_{i,1} < 0$, which can be realized by putting suitable bounds on the elements of $x^{(1)}(0)$, $x^{(2)}(0)$ and r. This procedure is conservative due to the nature of the triangular inequality. On the other hand, if the reference signal trajectories are known, one can check the inequality (31) numerically. We demonstrate the application of the latter approach in the simulation results sections.

For a constant reference input vector r, the inequality (31) can be simplified further. This is described in the following corollary.

Corollary 2. If, in addition to the conditions given in Corollary 1, the reference signals are constant, that is, $r_i(t) = R_i$, $i = 1, ..., \ell$, then the control signals v_i, $i = 1, ..., \ell$ are bounded by M_i, $i = 1, ..., \ell$, i.e. $|v_i| \leq M_i$, if the inequality

$$
\hat{W}_i \equiv \left| -\sum_{\omega=1}^{n-\ell} \sum_{j=1}^{n-\ell} \sum_{\kappa=1}^{\bar{n}} a_{2_{i,\omega}} c_{\omega,j_\kappa} e^{-h_{\omega,j_\kappa}t} x_j^{(1)}(0) - \sum_{\omega=1}^{n-\ell} \sum_{j=1}^{n-\ell} \sum_{\kappa=1}^{\bar{n}} \sum_{k=n-\ell+1}^{n} a_{2_{i,\omega}} c_{\omega,j_\kappa} a_{1_{j,k}} x_{k-n+\ell}^{(2)}(0) q_{\omega,j_\kappa}(t) \right.
$$
$$
\left. - \sum_{j=n-\ell+1}^{n} a_{2_{i,j}} \left(x_i^{(2)}(0) e^{-\bar{\lambda}t} + \frac{2}{\pi} R_i \tan^{-1}(\bar{\lambda}t) \right) - \bar{\lambda} x_{n-\ell+i}(0) e^{-\bar{\lambda}t} + \frac{2}{\pi} R_i \frac{\bar{\lambda}}{1 + \bar{\lambda}^2 t^2} \right|
$$
$$
+ \sum_{\omega=1}^{n-\ell} \sum_{j=1}^{n-\ell} \sum_{\kappa=1}^{\bar{n}} \left| \sum_{k=n-\ell+1}^{n} -a_{2_{i,\omega}} c_{\omega,j_\kappa} a_{1_{j,k}} R_{k-n+\ell} \right| \frac{1 - e^{-h_{\omega,j_\kappa}t}}{h_{\omega,j_\kappa}} \leq M_i - \rho_i, \quad i = 1, ..., \ell, \tag{33}
$$

where $q_{\omega,j_\kappa}(t)$ is defined in (32), is satisfied for all $t \geq 0$.
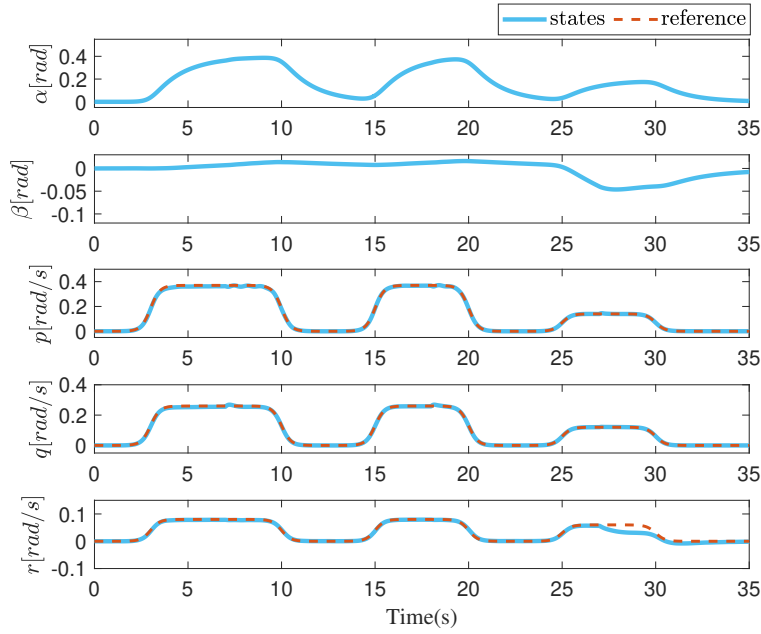
FIGURE 3 Time evolution of the aircraft states and the references, in the presence of actuator uncertainty. At $t = 7$s, $t = 18$s and $t = 27$s, 15%, 30% and 35%-70% losses of effectiveness are introduced, respectively.

Proof. The proof is similar to that of Corollary 1. □

Remark 6. The left hand side of the inequality (33) can be written as $|k_1 e^{-\bar{\lambda}t} + k_2 e^{-h_{\omega,j_\kappa}t} + k_3 \frac{\bar{\lambda}}{1+\bar{\lambda}^2 t^2} + k_4 \frac{2}{\pi}\tan^{-1}(\bar{\lambda}t) + k_5|$, where k_i, $i = 1, 2, ..., 5$ are the appropriate constant coefficients. Since all of the terms are monotonic functions, it's enough to check (33) at $t = 0$, $t = \infty$ and at the extremum points in between, if any. Extremum points can be found by taking the derivative and equating it to zero and finding the roots numerically.

4 | SIMULATION RESULTS

The Aerodata Model in Research Environment (ADMIRE), which represents the dynamics of an over-actuated aircraft model, is used to demonstrate the effectiveness of the proposed controller. The linearized ADMIRE model[29] is given as

$$\dot{x} = Ax + B_u u = Ax + B_v v_s,$$
$$v_s = Bu, \quad B_u = B_v B, \quad B_v = [0_{3\times 2} \ I_{3\times 3}]^T, \tag{34}$$

where $x = [\alpha \ \beta \ p \ q \ r]^T$ with α, β, p, q and r denote the angle of attack, sideslip angle, roll rate, pitch rate and yaw rate, respectively. The vector $u = [u_c \ u_{re} \ u_{le} \ u_r]^T$ represents the control surface deflections of canard wings, right and left elevons and the rudder. The position limits of the control surfaces are given as $u_c \in [-55, 25] \times \frac{\pi}{180} rad$, $u_{re}, u_{le}, u_r \in [-30, 30] \times \frac{\pi}{180} rad$. The actuators have first-order dynamics with a time constant of 0.05 s. The state and control matrices are provided by Härkegård et al.[29] To represent actuator loss of effectiveness and disturbance, a diagonal matrix Λ and a vector d_u, respectively, are introduced in the model (34) as

$$\dot{x} = Ax + B_u \Lambda u + B_u d_u = Ax + B_v v_s + B_v \bar{d}, \tag{35}$$
$$v_s = B\Lambda u + \bar{d}, \quad \bar{d} = Bd_u, \quad B_u = B_v B, \quad B_v = [0_{3\times 2} \ I_{3\times 3}]^T.$$

A sinusoidal function with amplitude of 0.1 and frequency of 1 rad/s is considered as the disturbance $\bar{d}$ in the simulation. Saturation limits are calculated as $M_1 = 1.4$, $M_2 = 1.4$ and $M_3 = 0.3$. Furthermore, the maximum and minimum range of the elements of θ_v for the projection algorithm are taken as $\theta_{v_{1,1}} \in [-0.0129, 0.0129]$, $\theta_{v_{1,2}} \in [0.0307, 0.5225]$, $\theta_{v_{1,3}} \in [-0.1357, 0.1371]$, $\theta_{v_{1,4}} \in [-0.212, 0]$, $\theta_{v_{2,1}} \in [-0.3149, -0.1113]$, $\theta_{v_{2,2}} \in [-0.217, -0.1416]$, $\theta_{v_{2,3}} \in [-0.0241, 0.2363]$, $\theta_{v_{2,4}} \in$
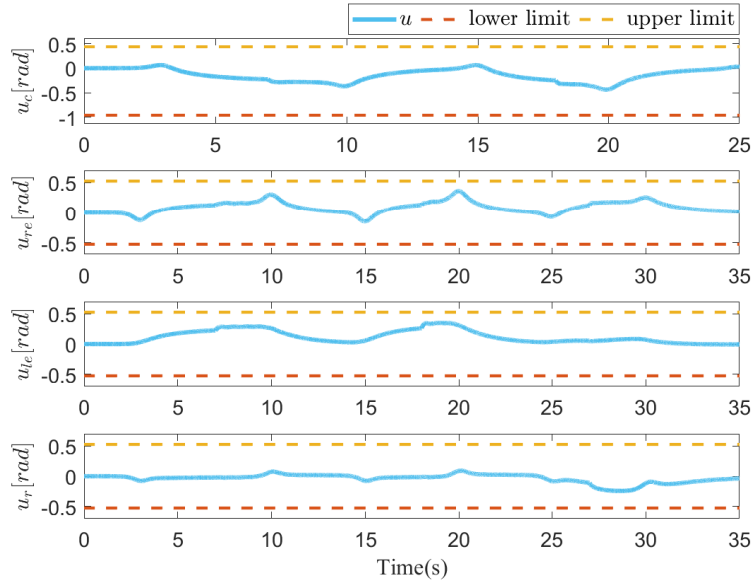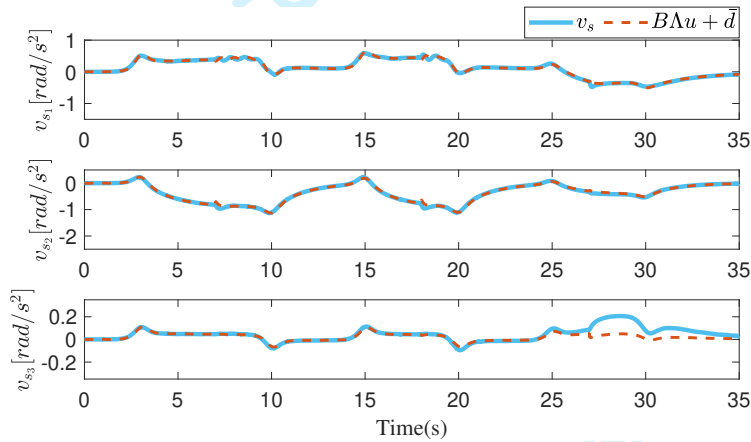
FIGURE 4 Time evolution of the control surfaces.

FIGURE 5 Control allocation performance.

$[-0.4162, -0.01]$, $\theta_{v_{3,1}} \in [0.1587, 0.1977]$, $\theta_{v_{3,2}} \in [0.0673, 0.0675]$, $\theta_{v_{3,3}} \in [-0.001, 0.001]$, and $\theta_{v_{3,4}} \in [-1.2755, -0.7641]$ (see Tohidi et al.[40] for how these values can be calculated). The proposed sliding mode controller is implemented using $\bar{\lambda} = 3$ (see (26)). To avoid chattering, the boundary layer approach[64] is used. The actuator loss of effectiveness is modeled as

$$\Lambda(t) = \begin{cases} diag(1,1,1,1) & for \ t \leq 7, \\ diag(0.85, 0.85, 0.85, 0.85) & for \ 7 < t \leq 18, \\ diag(0.7, 0.7, 0.7, 0.7) & for \ 18 < t \leq 27, \\ diag(0.65, 0.6, 0.65, 0.3) & for \ 27 < t. \end{cases}$$

Since $A_{1,1}$ in the ADMIRE model has distinct real eigenvalues, we can use Corollary 1, which requires (31) to be satisfied. The reference signals are chosen as

$$r_i(t) = \gamma_i \left(\frac{1}{1 + e^{-4(t-3)}} - \frac{1}{1 + e^{-4(t-10)}} + \frac{1}{1 + e^{-4(t-15)}} - \frac{1}{1 + e^{-4(t-20)}} \right) + \hat{\gamma}_i \left(\frac{1}{1 + e^{-4(t-25)}} - \frac{1}{1 + e^{-4(t-30)}} \right), \ i = 1, 2, 3,$$

$$(36)$$
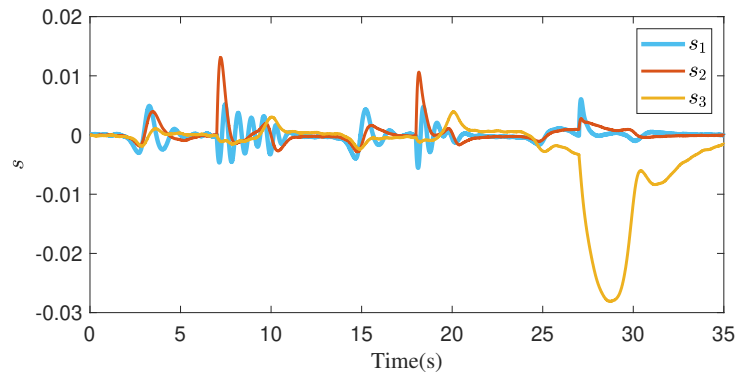
FIGURE 6 The evolution of the sliding surfaces.
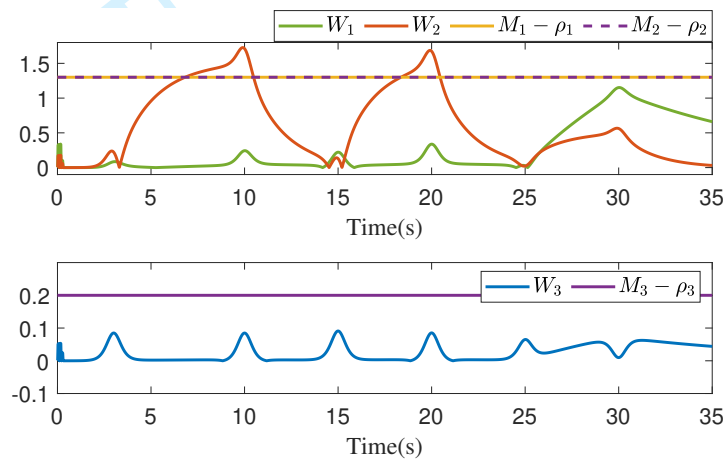
FIGURE 7 The case when the inequality (31) is not satisfied.

where $\gamma_1 = 0.37$, $\gamma_2 = 0.26$, $\gamma_3 = 0.08$, $\hat{\gamma}_1 = 0.14$, $\hat{\gamma}_2 = 0.12$ and $\hat{\gamma}_3 = 0.06$. It is seen in Figure 2 that the inequality (31) is satisfied for $i = 1, 2, 3$.

Figure 3 illustrates the time evolution of the states when 15% actuator loss of effectiveness occurs at $t = 7s$, 30% at $t = 18s$ and 35%-70% at $t = 27s$. The states remain bounded and p, q and r follow the reference signals. Figure 4 demonstrates the control surface deflections together with the saturation limits. The actuators stay within their limits. The performance of the control allocation is depicted in Figure 5. It shows that the control allocation determines the actuator input vector u in such a way that $B\Lambda u + \bar{d}$ follows the control signal v_s. Figure 6 shows the sliding surface trajectories, which tend to grow at the times of uncertainty injections but converge to a neighborhood of zero afterwards, without any chattering effect.

In order to show the robustness of the proposed method, we examine the case where the inequality (31) is violated. The violation is realized by setting the parameters γ_is and $\hat{\gamma}_i$s in (36) to $\gamma_1 = 0.4$, $\gamma_2 = 0.35$, $\gamma_3 = 0.09$, $\hat{\gamma}_1 = 0.14$, $\hat{\gamma}_2 = 0.12$ and $\hat{\gamma}_3 = 0.06$. It is seen in Figure 7 that the inequality (31) is violated by W_2. Figures 8–11 illustrate that even though (31) is not satisfied, the system remains stable, while tracking its references. Thus the controller is able to provide reasonable performance even when the inequality (31), which is a sufficient condition, is violated; the investigation of additional sufficient conditions, motivated by our simulation-based observations of the method's robustness, is left as a topic for continuing research.
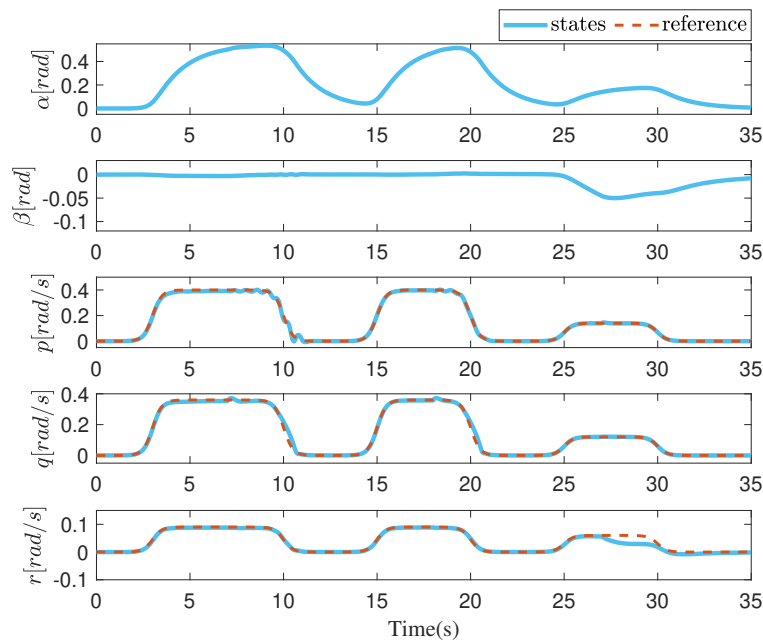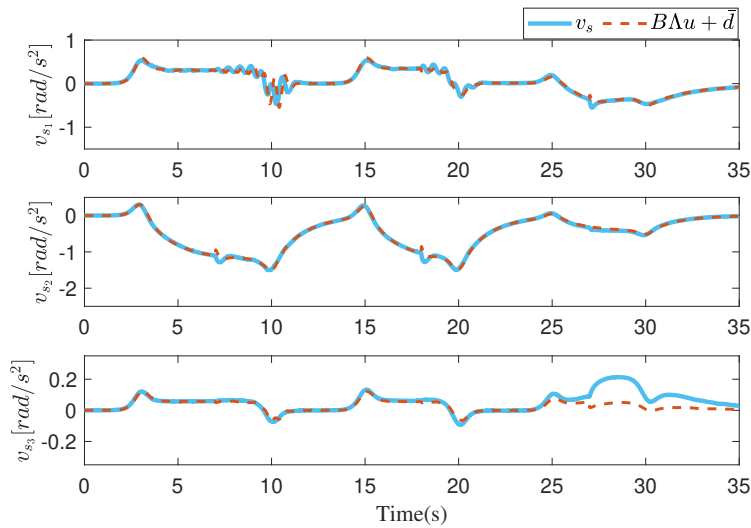
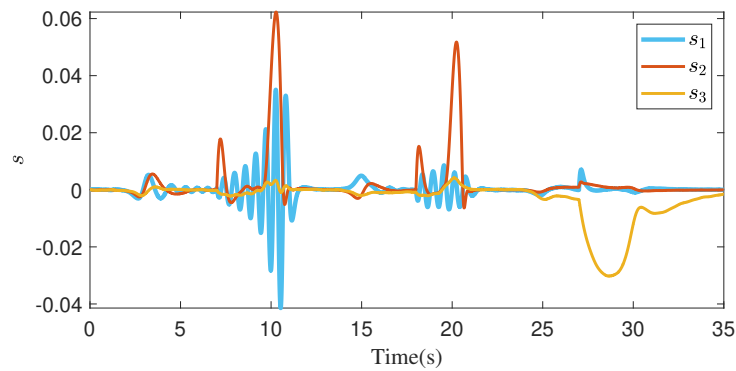**FIGURE 8** Time evolution of the states when (31) is violated.
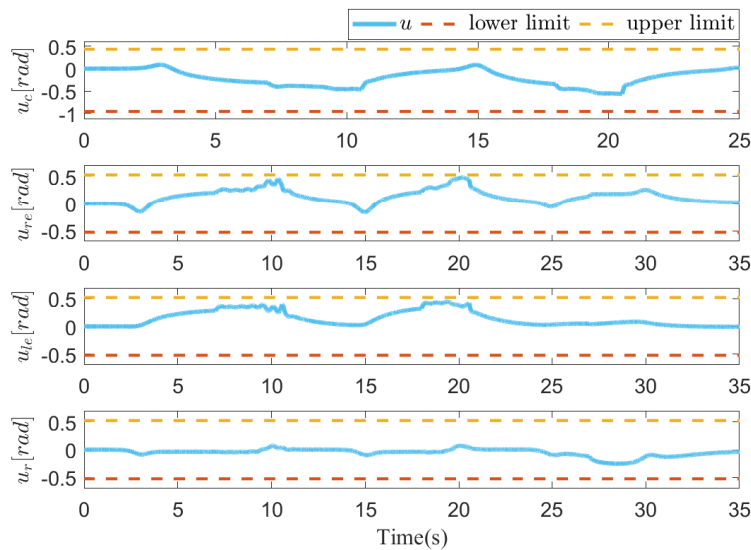
FIGURE 9 Time evolution of the control surfaces when (31) is violated.

5 | SUMMARY

In this paper, a sliding mode controller with a time-varying sliding surface is proposed to complement an adaptive control allocator for uncertain over-actuated systems with actuator saturation. Stability of the overall closed-loop system is shown using Lyapunov arguments. Simulation results with the ADMIRE model show the effectiveness of the proposed method.

FIGURE 10 Control allocation performance when (31) is violated. Control allocation signal v_s does not saturate, and therefore $v_s = v$ (see Figure 1).

FIGURE 11 The evolution of the sliding surfaces when (31) is violated.

DATA AVAILABILITY STATEMENT

Data sharing not applicable to this article as no datasets were generated or analyzed during the current study.

APPENDIX

A PROOF OF LEMMA 2

Rewriting (26) using the matrices in (16), we have

$$
\begin{bmatrix} v_1(t) \\ \vdots \\ v_\ell(t) \end{bmatrix} = - \begin{bmatrix} a_{2_{1,1}} & \cdots & a_{2_{1,(n-\ell)}} \\ \vdots & \ddots & \vdots \\ a_{2_{\ell,1}} & \cdots & a_{2_{\ell,(n-\ell)}} \end{bmatrix} \begin{bmatrix} x_1^{(1)}(t) \\ \vdots \\ x_{n-\ell}^{(1)}(t) \end{bmatrix} - \begin{bmatrix} a_{2_{1,(n-\ell+1)}} & \cdots & a_{2_{1,n}} \\ \vdots & \ddots & \vdots \\ a_{2_{\ell,(n-\ell+1)}} & \cdots & a_{2_{\ell,n}} \end{bmatrix} \begin{bmatrix} x_1^{(2)}(t) \\ \vdots \\ x_\ell^{(2)}(t) \end{bmatrix} - \bar\lambda e^{-\bar\lambda t} \begin{bmatrix} x_1^{(2)}(0) \\ \vdots \\ x_\ell^{(2)}(0) \end{bmatrix} + \frac{2}{\pi}\tan^{-1}(\bar\lambda t) \begin{bmatrix} \dot r_1(t) \\ \vdots \\ \dot r_\ell(t) \end{bmatrix}
$$

$$
+ \frac{2}{\pi}\frac{\bar\lambda}{1+\bar\lambda^2 t^2} \begin{bmatrix} r_1(t) \\ \vdots \\ r_\ell(t) \end{bmatrix} - \begin{bmatrix} \bar s_1(t) & 0 & 0 & \cdots & 0 \\ 0 & \bar s_2(t) & 0 & \cdots & 0 \\ \vdots & \vdots & \ddots & \cdots & \vdots \\ 0 & \cdots & 0 & \bar s_{\ell-1}(t) & 0 \\ 0 & \cdots & 0 & 0 & \bar s_\ell(t) \end{bmatrix} \begin{bmatrix} \rho_1 \\ \vdots \\ \rho_\ell \end{bmatrix}, \tag{A1}
$$

where $a_{2_{i,j}}$, $i=1,...,\ell$, $j=1,...,n-\ell$ are the elements of $A_{2,1}$, and $a_{2_{i,j}}$, $i=1,...,\ell$, $j=n-\ell+1,...,n$ are the elements of $A_{2,2}$. Also, $x_i^{(2)}$, r_i, $\dot r_i$ and ρ_i, $i=1,...,\ell$ are the elements of the vectors $x^{(2)}$, r, $\dot r$ and ρ, respectively, and $\bar s_i$ are the ith diagonal element of $\text{sign}_v\big(s(x^{(2)}(t), x^{(2)}(0), t)\big)$. Thus,

$$
v_i(t) = -\sum_{j=1}^{n-\ell} a_{2_{i,j}} x_j^{(1)}(t) - \sum_{j=n-\ell+1}^{n} a_{2_{i,j}} x_{j-n+\ell}^{(2)}(t) - \bar\lambda x_i^{(2)}(0)e^{-\bar\lambda t} + \frac{2}{\pi}\dot r_i(t)\tan^{-1}(\bar\lambda t) + \frac{2}{\pi} r_i(t)\frac{\bar\lambda}{1+\bar\lambda^2 t^2} - \bar s_i(t)\rho_i. \tag{A2}
$$

To ensure that $|v_i| \le M_i$ for $i=1,...,\ell$, the inequality

$$
\left| -\sum_{j=1}^{n-\ell} a_{2_{i,j}} x_j^{(1)}(t) - \sum_{j=n-\ell+1}^{n} a_{2_{i,j}} x_{j-n+\ell}^{(2)}(t) - \bar\lambda x_i^{(2)}(0)e^{-\bar\lambda t} + \frac{2}{\pi}\dot r_i(t)\tan^{-1}(\bar\lambda t) + \frac{2}{\pi} r_i(t)\frac{\bar\lambda}{1+\bar\lambda^2 t^2} - \bar s_i(t)\rho_i \right| \le M_i \tag{A3}
$$

should be satisfied for all $i=1,...,\ell$.

By considering the elements of $\Phi(t,t_0)$ as $\phi_{i,j}(t)$, $i=1,...,n-\ell$, $j=1,...,n-\ell$, with $t_0=0$, and substituting these in (23), we have

$$
\begin{bmatrix} x_1^{(1)}(t) \\ \vdots \\ x_{n-\ell}^{(1)}(t) \end{bmatrix} = \begin{bmatrix} \phi_{1,1}(t) & \cdots & \phi_{1,(n-\ell)}(t) \\ \vdots & \cdots & \vdots \\ \phi_{(n-\ell),1}(t) & \cdots & \phi_{(n-\ell),(n-\ell)}(t) \end{bmatrix} \begin{bmatrix} x_1^{(1)}(0) \\ \vdots \\ x_{n-\ell}^{(1)}(0) \end{bmatrix} + \int_0^t \begin{bmatrix} \phi_{1,1}(t-\eta) & \cdots & \phi_{1,(n-\ell)}(t-\eta) \\ \vdots & \cdots & \vdots \\ \phi_{(n-\ell),1}(t-\eta) & \cdots & \phi_{(n-\ell),(n-\ell)}(t-\eta) \end{bmatrix} \begin{bmatrix} g_1(\eta) \\ \vdots \\ g_{n-\ell}(\eta) \end{bmatrix} d\eta. \tag{A4}
$$

Remembering that $g(t) \equiv G_1 e^{-\bar\lambda(t-t_0)} + G_2(t)$, with $G_1 \equiv A_{1,2} x^{(2)}(t_0)$, and $G_2(t) \equiv \frac{2}{\pi} A_{1,2} r(t)\tan^{-1}(\bar\lambda(t-t_0))$, the elements of the vector $g(t)$ can be written as

$$
\begin{bmatrix} g_1(t) \\ \vdots \\ g_{n-\ell}(t) \end{bmatrix} = \begin{bmatrix} a_{1_{1,(n-\ell+1)}} & \cdots & a_{1_{1,n}} \\ \vdots & \ddots & \vdots \\ a_{1_{(n-\ell),(n-\ell+1)}} & \cdots & a_{1_{(n-\ell),n}} \end{bmatrix} \begin{bmatrix} x_1^{(2)}(0) \\ \vdots \\ x_\ell^{(2)}(0) \end{bmatrix} e^{-\bar\lambda t} + \frac{2}{\pi}\tan^{-1}(\bar\lambda t) \begin{bmatrix} a_{1_{1,(n-\ell+1)}} & \cdots & a_{1_{1,n}} \\ \vdots & \ddots & \vdots \\ a_{1_{(n-\ell),(n-\ell+1)}} & \cdots & a_{1_{(n-\ell),n}} \end{bmatrix} \begin{bmatrix} r_1(t) \\ \vdots \\ r_\ell(t) \end{bmatrix}. \tag{A5}
$$

Substituting (A5) into (A4), the ith element of the vector $x^{(1)}(t)$ can be written as

$$
x_i^{(1)}(t) = \sum_{j=1}^{n-\ell} \phi_{i,j}(t)x_j^{(1)}(0) + \int_0^t \left(\sum_{j=1}^{n-\ell} \phi_{i,j}(t-\eta) \left[\sum_{k=n-\ell+1}^{n} a_{1_{j,k}}\left(x_{k-n+\ell}^{(2)}(0)e^{-\bar\lambda\eta} + r_{k-n+\ell}(\eta)\frac{2}{\pi}\tan^{-1}(\bar\lambda\eta)\right) \right] \right) d\eta, \quad i=1,...,n-\ell,
$$

$$
\tag{A6}
$$

where $a_{1_{j,k}}$ refer to the elements of A_1. Substituting (A6) and the elements of $x^{(2)}$ (see (19)) in (A3), we have

$$
|v_i(t)| = \left| -\sum_{\omega=1}^{n-\ell}\sum_{j=1}^{n-\ell} a_{2_{i,\omega}}\phi_{\omega,j}(t)x_j^{(1)}(0) - \int_0^t \left(\sum_{\omega=1}^{n-\ell}\sum_{j=1}^{n-\ell} a_{2_{i,\omega}}\phi_{\omega,j}(t-\eta) \left[\sum_{k=n-\ell+1}^{n} a_{1_{j,k}}\left(x_{k-n+\ell}^{(2)}(0)e^{-\bar\lambda\eta} + r_{k-n+\ell}(\eta)\frac{2}{\pi}\tan^{-1}(\bar\lambda\eta)\right) \right] \right) d\eta \right.
$$

$$
\left. - \sum_{j=n-\ell+1}^{n} a_{2_{i,j}}\left(x_{j-n+\ell}^{(2)}(0)e^{-\bar\lambda t} + \frac{2}{\pi}r_{j-n+\ell}(t)\tan^{-1}(\bar\lambda t)\right) - \bar\lambda x_{n-\ell+i}(0)e^{-\bar\lambda t} + \frac{2}{\pi}\dot r_i(t)\tan^{-1}(\bar\lambda t) + \frac{2}{\pi}r_i(t)\frac{\bar\lambda}{1+\bar\lambda^2 t^2} - \bar s_i(x(t))\rho_i \right| \le M_i,
$$

$$
\tag{A7}
$$

for $i = 1, ..., \ell$. Using the triangle inequality, (30) is obtained.

B PROOF OF COROLLARY 1

The proof follows the same steps of the proof of Lemma 2 until (A6).

Substituting $\phi_{i,j}(t) = \sum_{\kappa=1}^{\bar{n}} c_{i,j_\kappa} e^{-h_{i,j_\kappa} t}$ into (A6), we obtain that

$$
\begin{aligned}
x_i^{(1)}(t) &= \sum_{j=1}^{n-\ell} \left(\sum_{\kappa=1}^{\bar{n}} c_{i,j_\kappa} e^{-h_{i,j_\kappa} t} \right) x_j^{(1)}(0) \\
&\quad + \int_0^t \left(\sum_{j=1}^{n-\ell} \left(\sum_{\kappa=1}^{\bar{n}} c_{i,j_\kappa} e^{-h_{i,j_\kappa}(t-\eta)} \right) \left[\sum_{k=n-\ell+1}^{n} a_{1_{j,k}} \left(x_{k-n+\ell}^{(2)}(0) e^{-\bar{\lambda}\eta} + r_{k-n+\ell}(\eta) \frac{2}{\pi} \tan^{-1}(\bar{\lambda}\eta) \right) \right] \right) d\eta \\
&= \sum_{j=1}^{n-\ell} \sum_{\kappa=1}^{\bar{n}} c_{i,j_\kappa} e^{-h_{i,j_\kappa} t} x_j^{(1)}(0) + \int_0^t \sum_{j=1}^{n-\ell} \sum_{\kappa=1}^{\bar{n}} \sum_{k=n-\ell+1}^{n} c_{i,j_\kappa} e^{-h_{i,j_\kappa}(t-\eta)} a_{1_{j,k}} \left(x_{k-n+\ell}^{(2)}(0) e^{-\bar{\lambda}\eta} + r_{k-n+\ell}(\eta) \frac{2}{\pi} \tan^{-1}(\bar{\lambda}\eta) \right) d\eta \\
&= \sum_{j=1}^{n-\ell} \sum_{\kappa=1}^{\bar{n}} c_{i,j_\kappa} e^{-h_{i,j_\kappa} t} x_j^{(1)}(0) + \sum_{j=1}^{n-\ell} \sum_{\kappa=1}^{\bar{n}} \sum_{k=n-\ell+1}^{n} \left(\int_0^t c_{i,j_\kappa} e^{-h_{i,j_\kappa}(t-\eta)} a_{1_{j,k}} x_{k-n+\ell}^{(2)}(0) e^{-\bar{\lambda}\eta} d\eta \right. \\
&\quad \left. + \int_0^t c_{i,j_\kappa} e^{-h_{i,j_\kappa}(t-\eta)} a_{1_{j,k}} r_{k-n+\ell}(\eta) \frac{2}{\pi} \tan^{-1}(\bar{\lambda}\eta) d\eta \right), \quad i = 1, ..., n-\ell.
\end{aligned}
\tag{B8}
$$

Substituting (19) with $t_0 = 0$ and (B8) in (A3), we get

$$
\begin{aligned}
|v_i(t)| = \left| -\sum_{\omega=1}^{n-\ell} \sum_{j=1}^{n-\ell} \sum_{\kappa=1}^{\bar{n}} a_{2_{i,\omega}} c_{\omega,j_\kappa} e^{-h_{\omega,j_\kappa} t} x_j^{(1)}(0) - \sum_{\omega=1}^{n-\ell} \sum_{j=1}^{n-\ell} \sum_{\kappa=1}^{\bar{n}} \sum_{k=n-\ell+1}^{n} \left(\int_0^t a_{2_{i,\omega}} c_{\omega,j_\kappa} e^{-h_{\omega,j_\kappa}(t-\eta)} a_{1_{j,k}} x_{k-n+\ell}^{(2)}(0) e^{-\bar{\lambda}\eta} d\eta \right. \right. \\
\left. + \int_0^t a_{2_{i,\omega}} c_{\omega,j_\kappa} e^{-h_{\omega,j_\kappa}(t-\eta)} a_{1_{j,k}} r_{k-n+\ell}(\eta) \frac{2}{\pi} \tan^{-1}(\bar{\lambda}\eta) d\eta \right) - \sum_{j=n-\ell+1}^{n} a_{2_{i,j}} \left(x_i^{(2)}(0) e^{-\bar{\lambda}t} + \frac{2}{\pi} r_i(t) \tan^{-1}(\bar{\lambda}t) \right) \\
\left. - \bar{\lambda} x_{n-\ell+i}(0) e^{-\bar{\lambda}t} + \frac{2}{\pi} \dot{r}_i(t) \tan^{-1}(\bar{\lambda}t) + \frac{2}{\pi} r_i(t) \frac{\bar{\lambda}}{1 + \bar{\lambda}^2 t^2} - \bar{s}_i(x(t)) \rho_i \right| \leq M_i, \quad i = 1, ..., \ell.
\end{aligned}
\tag{B9}
$$

Defining $q_{\omega,j_\kappa}(t)$ as

$$
q_{\omega,j_\kappa}(t) = \int_0^t e^{-h_{\omega,j_\kappa}(t-\eta)} e^{-\bar{\lambda}\eta} d\eta = \begin{cases} t e^{-h_{\omega,j_\kappa} t}, & \bar{\lambda} = h_{\omega,j_\kappa}, \\ \frac{e^{-\bar{\lambda}t} - e^{-h_{\omega,j_\kappa} t}}{h_{\omega,j_\kappa} - \bar{\lambda}}, & \bar{\lambda} \neq h_{\omega,j_\kappa}, \end{cases}
\tag{B10}
$$

remembering that $\bar{s}_i$ is either 1 or -1, and using the triangle inequality, we can rewrite (B9) as (31).

References

1. Yildiz Y, Kolmanovsky I. Stability properties and cross-coupling performance of the control allocation scheme CAPIO. *Journal of Guidance, Control, and Dynamics* 2011; 34(4): 1190–1196.

2. Ducard GJJ. *Fault-tolerant flight control and guidance systems: Practical methods for small unmanned aerial vehicles*. Springer Science & Business Media; 2009.

3. Bodson M. Evaluation of optimization methods for control allocation. *Journal of Guidance, Control, and Dynamics* 2002; 25(4): 703–711.

4. Liao F, Lum KY, Wang J, Benosman M. Adaptive control allocation for non-linear systems with internal dynamics. *IET control theory & applications* 2010; 4(6): 909–922.

5. Shen Q, Wang D, Zhu S, Poh EK. Inertia-free fault-tolerant spacecraft attitude tracking using control allocation. *Automatica* 2015; 62: 114–121.

6. Yildiz Y, Kolmanovsky I. Implementation of CAPIO for composite adaptive control of cross-coupled unstable aircraft. *Infotech@ Aerospace;* 2011.

7. Acosta DM, Yildiz Y, Craun RW, et al. Piloted evaluation of a control allocation technique to recover from pilot-induced oscillations. *Journal of Aircraft* 2014; 52(1): 130–140.

8. Shen Q, Wang D, Zhu S, Poh EK. Robust control allocation for spacecraft attitude tracking under actuator faults. *IEEE Transactions on Control Systems Technology* 2017; 25(3): 1068–1075.

9. Sadeghzadeh I, Chamseddine A, Zhang Y, Theilliol D. Control allocation and re-allocation for a modified quadrotor helicopter against actuator faults. *IFAC Proceedings Volumes* 2012; 45(20): 247–252.

10. Tohidi SS, Yildiz Y, Kolmanovsky I. Pilot Induced Oscillation Mitigation for Unmanned Aircraft Systems: An Adaptive Control Allocation Approach. *IEEE Conference on Control Technology and Applications* 2018: 343–348.

11. Podder TK, Sarkar N. Fault-tolerant control of an autonomous underwater vehicle under thruster redundancy. *Robotics and Autonomous Systems* 2001; 34(1): 39–52.

12. Gierusz W, Tomera M. Logic thrust allocation applied to multivariable control of the training ship. *Control Engineering Practice* 2006; 14(5): 511–524.

13. Johansen TA, Fuglseth TP, Tøndel P, Fossen TI. Optimal constrained control allocation in marine surface vessels with rudders. *Control Engineering Practice* 2008; 16(4): 457–464.

14. Chen M, Ge SS, How BVE, Choo YS. Robust adaptive position mooring control for marine vessels. *IEEE Transactions on Control Systems Technology* 2013; 21(2): 395–409.

15. Sørensen AJ. A survey of dynamic positioning control systems. *Annual Reviews in Control* 2011; 35(1): 123–136.

16. Corradini ML, Cristofaro A. A nonlinear fault-tolerant thruster allocation architecture for underwater remotely operated vehicles. *IFAC-PapersOnLine* 2016; 49(23): 285–290.

17. Tjønnås J, Johansen TA. Stabilization of automotive vehicles using active steering and adaptive brake control allocation. *IEEE Transactions on Control Systems Technology* 2010; 18(3): 545–558.

18. Temiz O, Cakmakci M, Yildiz Y. A fault tolerant vehicle stability control using adaptive control allocation. *Dynamic Systems and Control Conference;* 2018.

19. Temiz O, Cakmakci M, Yildiz Y. A fault tolerant integrated vehicle stability control using adaptive control allocation. *arXiv preprint arXiv:2008.05697* 2020.

20. Tohidi SS, Khaki Sedigh A. Adaptive fault tolerance in automotive vehicle using control allocation based on the pseudo inverse along the null space for yaw stabilization. *The 3rd International Conference on Control, Instrumentation, and Automation;* 2013: 174–179.

21. Taghirad HD, Bedoustani YB. An analytic-iterative redundancy resolution scheme for cable-driven redundant parallel manipulators. *IEEE Transactions on Robotics* 2011; 27(6): 1137–1143.

22. Bouarfa A, Bodson M, Fadel M. A fast active-balancing method for the 3-phase multilevel flying capacitor inverter derived from control allocation theory. *IFAC-PapersOnLine* 2017; 50(1): 2113–2118.

23. Raoufat ME, Tomsovic K, Djouadi SM. Dynamic control allocation for damping of inter-area oscillations. *IEEE Transactions on Power Systems* 2017; 32(6): 4894–4903.

24. Durham WC. Constrained control allocation. *Journal of Guidance, control, and Dynamics* 1993; 16(4): 717–725.

25. Durham W, Bordignon KA, Beck R. *Aircraft Control allocation*. Springer Science & Business Media; 2017.

26. Alwi H, Edwards C. Fault tolerant control using sliding modes with on-line control allocation. *Automatica* 2008; 44(7): 1859–1866.

27. Tohidi SS, Khaki Sedigh A, Buzorgnia D. Fault tolerant control design using adaptive control allocation based on the pseudo inverse along the null space. *International Journal of Robust and Nonlinear Control* 2016; 26(16): 3541–3557.

28. Petersen JA, Bodson M. Constrained quadratic programming techniques for control allocation. *IEEE Transactions on Control Systems Technology* 2006; 14(1): 91–98.

29. Härkegård O, Glad ST. Resolving actuator redundancy-optimal control vs. control allocation. *Automatica* 2005; 41(1): 137–144.

30. Casavola A, Garone E. Fault-tolerant adaptive control allocation schemes for overactuated systems. *International Journal of Robust and Nonlinear Control* 2010; 20(17): 1958–1980.

31. Härkegård O. Efficient active set algorithms for solving constrained least squares problems in aircraft control allocation. *IEEE Conference on Decision and Control;* 2002: 1295–1300.

32. Yildiz Y, Kolmanovsky IV. A control allocation technique to recover from pilot-induced oscillations (CAPIO) due to actuator rate limiting. *American Control Conference;* 2010: 516–523.

33. Yildiz Y, Kolmanovsky IV, Acosta D. A control allocation system for automatic detection and compensation of phase shift due to actuator rate limiting. *American Control Conference;* 2011: 444–449.

34. Zaccarian L. Dynamic allocation for input redundant control systems. *Automatica* 2009; 45(6): 1431–1438.

35. Tjønnås J, Johansen TA. Adaptive control allocation. *Automatica* 2008; 44(11): 2754–2765.

36. Falconí GP, Holzapfel F. Adaptive fault tolerant control allocation for a hexacopter system. *American Control Conference (ACC);* 2016: 6760–6766.

37. Tohidi SS, Yildiz Y, Kolmanovsky I. Fault tolerant control for over-actuated systems: An adaptive correction approach. *American Control Conference;* 2016: 2530–2535.

38. Tohidi SS, Yildiz Y, Kolmanovsky I. Adaptive Control Allocation for Over-Actuated Systems with Actuator Saturation. *IFAC-PapersOnLine* 2017; 50(1): 5492–5497.

39. Galeani S, Sassano M. Data-Driven Dynamic Control Allocation for Uncertain Redundant Plants. *IEEE Conference on Decision and Control;* 2018: 5494–5499.

40. Tohidi SS, Yildiz Y, Kolmanovsky I. Adaptive control allocation for constrained systems. *Automatica* 2020; 121: 109161.

41. Johansen TA, Fossen TI. Control allocation—a survey. *Automatica* 2013; 49(5): 1087–1103.

42. Tarbouriech S, Garcia G, Silva Jr. JM, Queinnec I. *Stability and stabilization of linear systems with saturating actuators*. Springer Science & Business Media; 2011.

43. Buffington JM, Enns DF. Lyapunov stability analysis of daisy chain control allocation. *Journal of Guidance, Control, and Dynamics* 1996; 19(6): 1226–1230.

44. Molnar L, Omerdic E, Toal D. Guidance, navigation and control system for the Tethra unmanned underwater vehicle. *International Journal of Control* 2007; 80(7): 1050–1076.

45. Safa A, Baradarannia M, Kharrati H, Khanmohammadi S. Robust attitude tracking control for a rigid spacecraft under input delays and actuator errors. *International Journal of Control* 2019; 92(5): 1183–1195.

46. Naskar AK, Patra S, Sen S. New control allocation algorithms in fixed point framework for overactuated systems with actuator saturation. *International Journal of control* 2017; 90(2): 348–356.

47. Naderi M, Sedigh AK, Johansen TA. Guaranteed feasible control allocation using model predictive control. *Control Theory and Technology* 2019; 17(3): 252–264.

48. Tohidi SS, Yildiz Y. Handling actuator magnitude and rate saturation in uncertain over-actuated systems: A modified projection algorithm approach. *International Journal of Control* 2020: 1–24.

49. Ríos H, Kamal S, Fridman LM, Zolghadri A. Fault tolerant control allocation via continuous integral sliding-modes: a HOSM-observer approach. *Automatica* 2015; 51: 318–325.

50. Chen L, Edwards C, Alwi H, Sato M. Flight evaluation of a sliding mode online control allocation scheme for fault tolerant control. *Automatica* 2020; 114: 108829.

51. Steinberger M, Castillo I, Horn M, Fridman L. Robust output tracking of constrained perturbed linear systems via model predictive sliding mode control. *International Journal of Robust and Nonlinear Control* 2020; 30(3): 1258–1274.

52. Incremona GP, Ferrara A, Magni L. Hierarchical model predictive/sliding mode control of nonlinear constrained uncertain systems. *IFAC-PapersOnLine* 2015; 48(23): 102–109.

53. Rubagotti M, Raimondo DM, Ferrara A, Magni L. Robust model predictive control with integral sliding mode in continuous-time sampled-data nonlinear systems. *IEEE Transactions on Automatic Control* 2010; 56(3): 556–570.

54. Raimondo DM, Rubagotti M, Jones CN, Magni L, Ferrara A, Morari M. Multirate sliding mode disturbance compensation for model predictive control. *International Journal of Robust and Nonlinear Control* 2015; 25(16): 2984–3003.

55. Golkani MA, Seeber R, Reichhartinger M, Horn M. Lyapunov-based saturated continuous twisting algorithm. *International Journal of Robust and Nonlinear Control* 2021; 31(9): 3513–3527.

56. Ferrara A, Incremona GP, Regolin E. Optimization-based adaptive sliding mode control with application to vehicle dynamics control. *International Journal of Robust and Nonlinear Control* 2019; 29(3): 550–564.

57. Seeber R, Reichhartinger M. Conditioned Super-Twisting Algorithm for systems with saturated control action. *Automatica* 2020; 116: 108921.

58. Seeber R, Horn M. Guaranteeing disturbance rejection and control signal continuity for the saturated super-twisting algorithm. *IEEE Control Systems Letters* 2019; 3(3): 715–720.

59. Corradini ML, Cristofaro A, Orlando G. Robust stabilization of multi input plants with saturating actuators. *IEEE Transactions on Automatic Control* 2010; 55(2): 419–425.

60. Tohidi SS, Yildiz Y, Kolmanovsky I. Sliding mode control for over-actuated systems with adaptive control allocation and its applications to flight control. *2021 IEEE Conference on Control Technology and Applications (CCTA)* 2021: 765–770.

61. Eugene L, Kevin W, Howe D. *Robust and adaptive control with aerospace applications*. Springer London; 2013.

62. Stevens BL, Lewis FL, Johnson EN. *Aircraft control and simulation: dynamics, controls design, and autonomous systems*. John Wiley & Sons; 2015.

63. Antsaklis PJ, Michel AN. *Linear systems*. Springer Science & Business Media; 2006.

64. Slotine JJE, Li W. *Applied nonlinear control*. Prentice hall Englewood Cliffs, NJ; 1991.

65. Utkin V, Shi J. Integral sliding mode in systems operating under uncertainty conditions. *Proceedings of 35th IEEE conference on decision and control;* 1996: 4591–4596.

66. Nechepurenko YM. Bounds for the matrix exponential based on the Lyapunov equation and limits of the Hausdorff set. *Computational mathematics and mathematical physics* 2002; 42(2): 125–134.

Novelty file

Explain why the paper is relevant to the journal as described in the aims and scope?

This paper proposes a sliding mode controller with a time-varying sliding surface to complement adaptive control allocation for uncertain over-actuated systems. Sliding mode controllers are categorized as robust and nonlinear controllers, which are relevant to the aims of this journal for the development of analysis and design techniques for uncertain systems.

Explain why the theoretical contributions in the paper are novel?

In this paper, a novel robust controller is proposed which can handle the adaptive control allocation error, actuator saturation and external disturbances for systems with redundant actuators. No similar controller exists in the literature that has the ability to handle actuator saturation and disturbances in the presence of an adaptive control allocator. The cooperation of the proposed sliding mode controller and adaptive control allocation guarantees stability and reference tracking for over-actuated systems in the presence of uncertainty.

Provide a list of keywords that must correspond with the topics covered by the journal and dealt with in the paper.

sliding mode control, adaptive control allocation

Dear Professor Fridman,

We would like to thank you, the associate editor and the reviewers for the valuable comments and suggestions. In this letter, we address the reviewers' comments in the following form:

"Reviewer comments are quoted in this form."

Our response is written in this font.

<u>Specific actions taken in the revised manuscript are emphasized in this font.</u>

Text modifications in the revised manuscript are written in this font.

Please see the next page.

Associate Editor's Report:

"The main point is to clarify the contribution with respect to the conference paper mentioned by reviewer 1."

Reviewer 1 suggested using different simulation scenarios to avoid replica of the simulation results of the conference version. Therefore, we have changed the simulation scenarios in the revised version. Specifically, we have changed the simulation time, reference signals (36) and the actuator loss of effectiveness. With these modifications, the new figures are now substantively different from the ones in the conference paper.

Reviewer 1

"Despite the efforts done by the authors to clarify the contribution, it is not clear to me if the simulations are different. I checked again the conference paper, and in the latter Figures 3,4,5 and 6 looks exactly the same. I believe that, if differences are present, they should be highlighted, otherwise I think that a different simulation scenario and conditions should be considered to avoid a replica of the simulation results of the conference paper. For the rest I do not have other comments."

In the revised manuscript, we have changed the simulation scenarios. Specifically, we have changed the simulation time, reference signals (36) and the actuator loss of effectiveness. With these modifications, the new figures are now substantively different from the ones in the conference paper.

Reviewer: 2

"I only have some minors comments:

1. The authors are encouraged to double-check the manuscript. There are still some misprints."

We have double-checked the document, as the reviewer suggested, and corrected a few misprints that we have found.

"2. There is a typo in line 50 on page 11 in the current version."

We have checked the specified page but could not find a typo. We have, however, corrected a few misprints that we have found elsewhere.

1
2
3
4
5
6
7
8
9
10
11
12
13
14
15
16
17
18
19
20
21
22
23
24
25
26
27
28
29
30
31
32
33
34
35
36
37
38
39
40
41
42
43
44
45
46
47
48
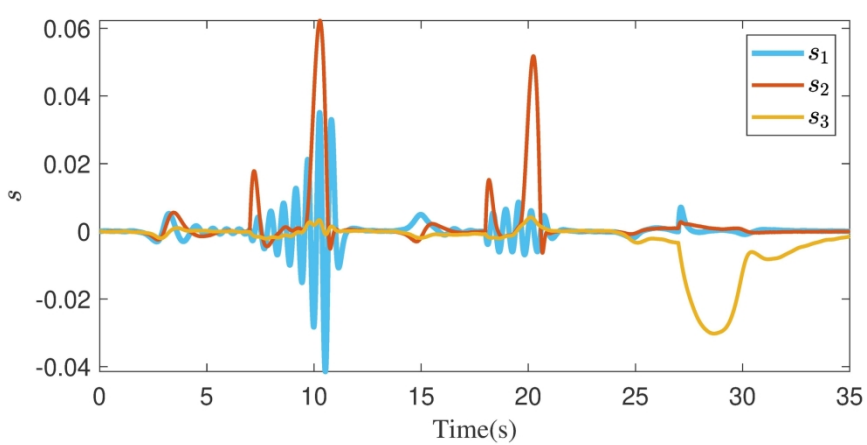49
50
51
52
53
54
55
56
57
58
59
60

"3. Regarding my previous comment 3, I still consider that it is not beneficial for the main contribution to show the second example in the simulation results. In Figs. 3 and 8, if we analyzed them, it is possible to notice the behaviour of the states is practically the same, then, the fulfilment of the inequality (31) is not necessary to obtain a good closed-loop performance."

We agree with the reviewer that (31) is not a necessary condition. The point of the second example is exactly that. Equation (31) is a sufficient condition and the controller can still provide reasonable performance even in the case when (31) is not satisfied. The example is important for potential users of our method since it shows that the controller is still able to provide reasonable performance even if the sufficient condition that we derived does not hold. In the revised version, we have modified the simulation results to make them different from the conference version. However, the conclusion that the controller is able to provide reasonable performance even if our sufficient condition does not hold is still valid for this simulation. Following the description of the example <u>we have also added a comment that the investigation of additional sufficient conditions, motivated by our simulation-based observations of our method's robustness, is left as a topic for continuing research.</u>

1
2
3
4
5
6
7
8
9
10
11
12
13
14
15
16
17
18
19
20
21
22
23
24
25
26
27
28
29
30
31
32
33
34
35
36
37
38
39
40
41
42
43
44
45
46
47
48
49
50
51
52
53
54
55
56
57
58
59
60
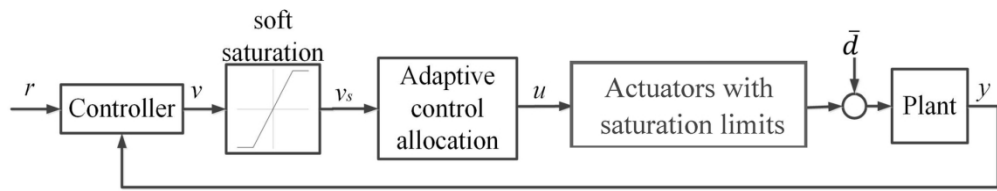
FIGURE 1: Block diagram of the closed loop system.

172x39mm (300 x 300 DPI)

FIGURE 2: Validation of the inequality (31).

203x101mm (300 x 300 DPI)

FIGURE 11: The evolution of the sliding surfaces when (31) is violated.
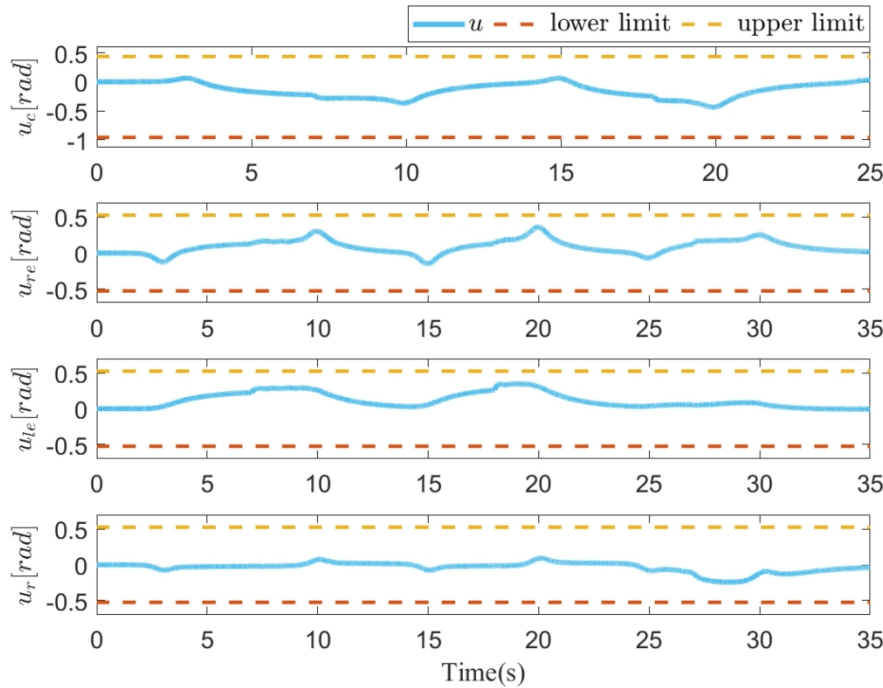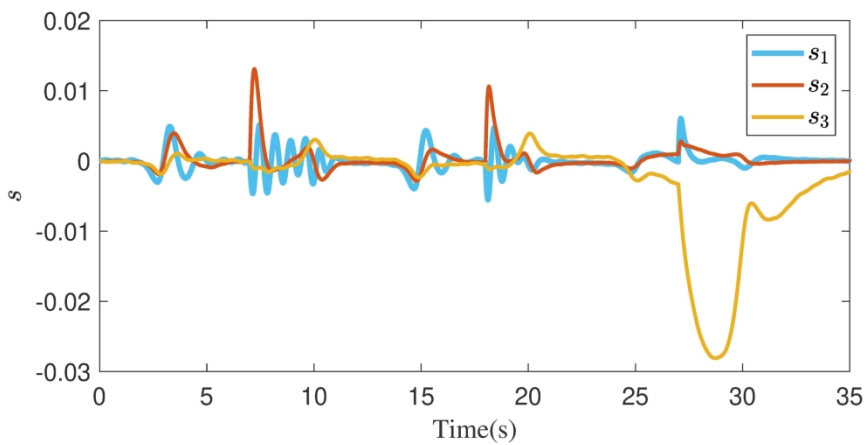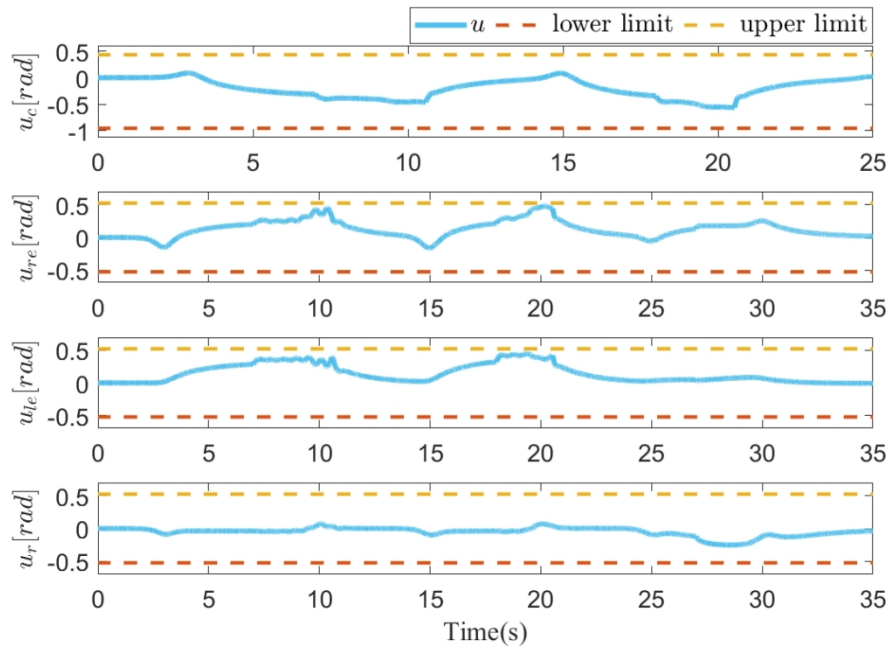
203x101mm (300 x 300 DPI)
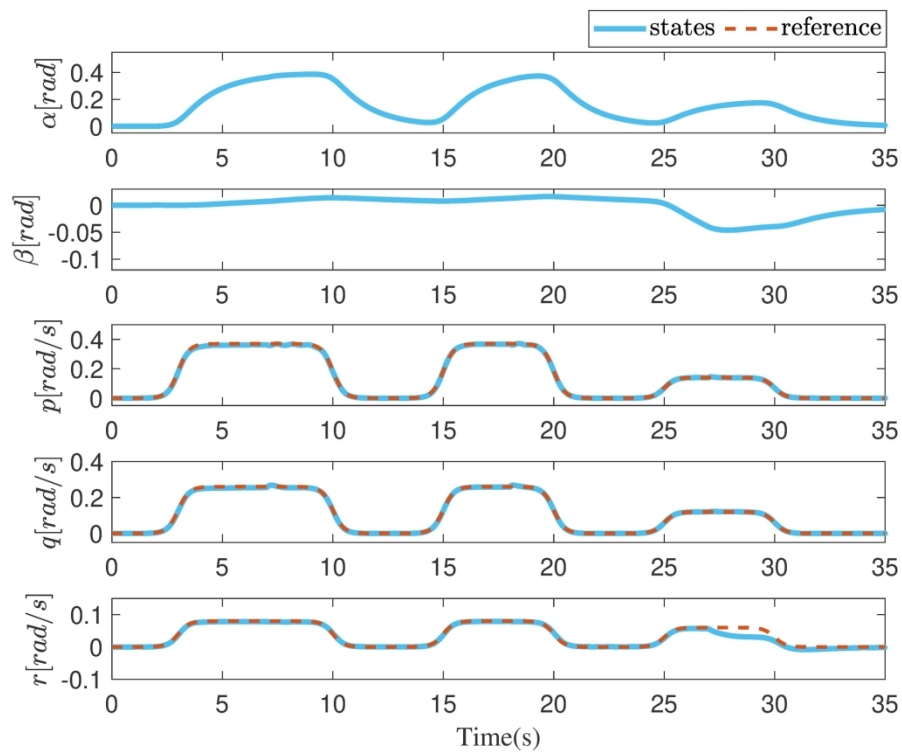
FIGURE 3: Time evolution of the aircraft states and the references, in the presence of actuator uncertainty. At τ = 7s, τ = 18s and τ = 27, 15%, 30% and 35%-70% losses of effectiveness are introduced, respectively.

203x160mm (300 x 300 DPI)

1
2
3
4
5
6
7
8
9
10
11
12
13
14
15
16
17
18
19
20
21
22
23
24
25
26
27
28
29
30
31
32
33
34
35
36
37
38
39
40
41
42
43
44
45
46
47
48
49
50
51
52
53
54
55
56
57
58
59
60

FIGURE 4: Time evolution of the control surfaces.

203x144mm (300 x 300 DPI)
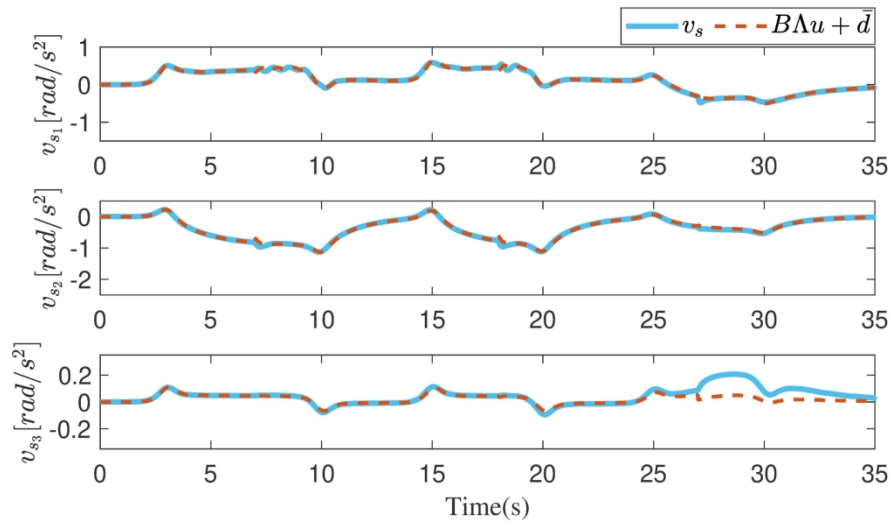
FIGURE 5: Control allocation performance.

203x104mm (300 x 300 DPI)

FIGURE 6: The evolution of the sliding surfaces.

203x101mm (300 x 300 DPI)
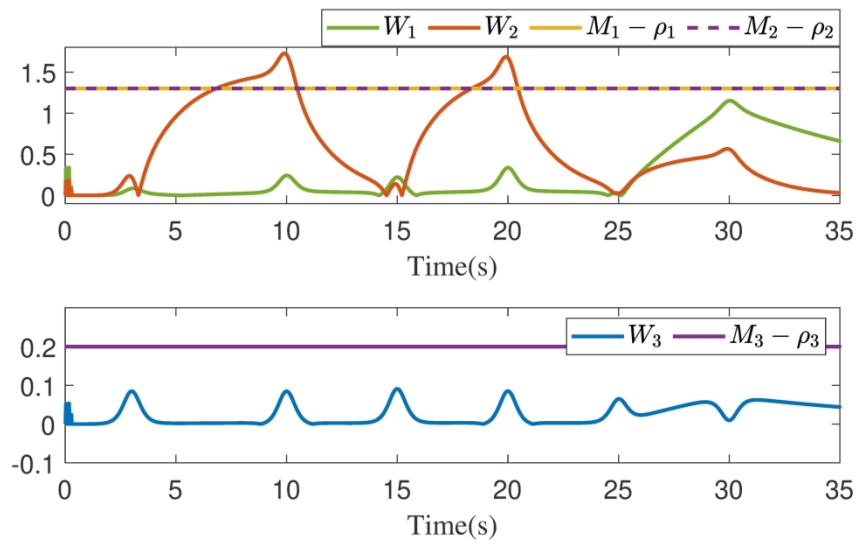
FIGURE 7: The case when the inequality (31) is not satisfied.

203x111mm (300 x 300 DPI)
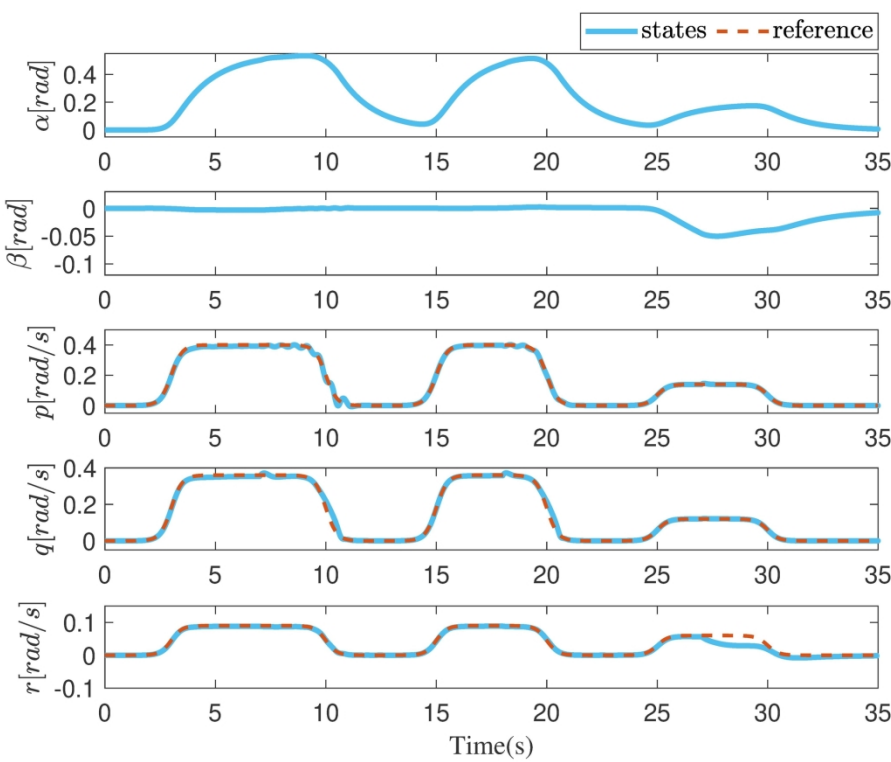
FIGURE 8: Time evolution of the states when (31) is violated.

203x162mm (300 x 300 DPI)

FIGURE 9: Time evolution of the control surfaces when (31) is violated.

203x135mm (300 x 300 DPI)
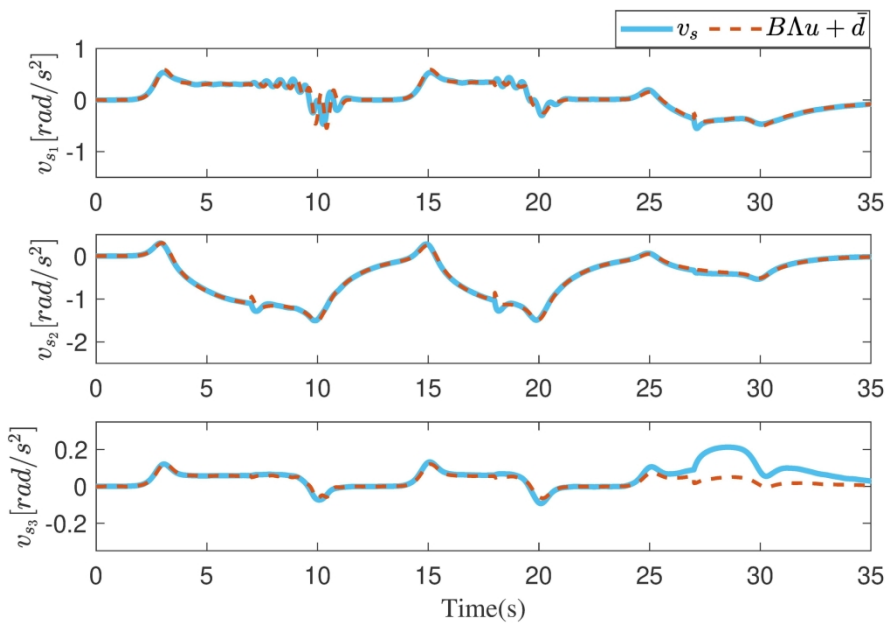
FIGURE 10: Control allocation performance when (31) is violated. Control allocation signal ���� does not saturate, and therefore ���� = �� (see Figure 1).

203x126mm (300 x 300 DPI)